ULTRASONIC SCANNER FOR IN VIVO DETECTION OF ULTRASONICALLY INDUCED CAVITATION ACTIVITY

BY

CLARENCE RAYMOND REILLY

B.S., University of Illinois, 1984

THESIS

Submitted in partial fulfillment of the requirements
for the degree of Master of Science in Electrical Engineering
in the Graduate College of the
University of Illinois at Urbana-Champaign, 1986

Urbana, Illinois

Ackowledgements

I wish first to express my gratitude to my family, especially my wife Whitney, for their support and encouragement during my education and the completion of this research. I dedicate this work to you.

I express my thanks to Dr. Leon A. Frizzell who helped guide this research, to Chong Lee for his helpful suggestions, to Joseph Cobb and Billy McNeill for their technical assistance during the system modification, to Robert Cicone for the care of the laboratory animals, and to Wanda Elliott for her assistance during the preparation of this thesis.

TABLE OF CONTENTS

CHAPTER 1

INTRODUCTION

1.1. INTRODUCTION

Ultrasound is one of the most widely used techniques in medicine today. Its primary use is in diagnosis, where it is employed in virtually every region of the body. Pulse echo and continuous wave (cw) Doppler techniques are the most common types of diagnostic ultrasound. Static and dynamic imaging of the soft tissues of the body using pulse echo techniques helps detect abnormalities such as cardiac disorders, fetal anomalies, and tumors. The popularity of pulse echo systems has increased with the development of real time capability and improved resolution. Doppler techniques utilize information contained in the frequency shift of signals reflected from moving particles to directly measure blood flow velocities, and are being applied to the diagnosis of a wide range of clinical problems.

Surgical applications of ultrasound employ intensities of 10 W/cm^2 or greater to destroy tissues. Acoustic microscopes using frequencies in the GHz range are used in medical research when the acoustic properties of the specimen can provide more, or different, information than the optical properties.

Various biological effects due to continuous and pulsed exposure to ultrasound have been reported. The reported biological effects were attributed to a combination of thermal, stress, and cavitation effects as defined by Nyborg (1978). Biological effects are most likely due to a combination of these mechanisms, but are usually classified according to the primary

mechanism involved. Cavitation is the probable mechanism when the application of excess hydrostatic pressure eliminates or reduces the biological effect, and when lower frequencies are, in general, more effective than higher frequencies in producing the effects . Cavitation can affect biological systems by virtue of thermal, mechanical, or chemical mechanisms. Cavitation bubbles cause scattering and increased heating. If a bubble collapses, as with transient cavitation, a shock wave may be generated which can produce severe mechanical damage. The high temperatures in the minimum volume state during collapse can cause water vapor in the bubble to dissociate into highly reactive free radicals capable of producing chemical changes in the medium and which can result in sonoluminescence.

Attenuation, which includes absorption and scattering, is the decrease in amplitude as the sound travels through the tissue. The absorption of ultrasonic energy resulting in heating of tissues is a fairly well understood mechanism for damage. Biological effects are classified as thermal when the effect can be observed if the temperature is elevated by the same amount using other means (NCRP, 1983). Thermal effects often have a well defined threshold where change occurs reproducibly above a narrow critical range of temperatures.

Mechanically mediated biological effects can be correlated to the spatial and temporal distributions of various parameters descriptive of mechanical stress, strain, and motion (NCRP, 1983). These parameters include pressure, tension, shearing stress, expansion, compression, velocity, and acceleration. Radiation force, radiation torque, and acoustic streaming are

nonthermal second order mechanisms responsible for some of the biological effects that have been observed (NCRP, 1983). Radiation force is the steady force exerted on objects in a sound field, which may cause translational motion. A standing wave field in a suspension of small particles can produce banding according to radiation force theory. Also, pulsating bubbles exert an attractive force on particles in their vicinity. In cell suspensions, cells can be pulled into regions of high stress where damage is likely to occur. Rotary motion of objects in the sound field may be the result of a steady radiation torque. Radiation torque acts on the medium itself and, in fluid, gives rise to steady circulatory flow known as acoustic streaming (Nyborg, 1965). Oscillation of a bubble, especially if it exists near a solid boundary, is likely to produce acoustic microstreaming, i.e., streaming on a microscopic scale. The expected velocity of near-boundary acoustic streaming and the radiation force on small particles are proportional to the gradient of the square of the first order velocity field (Nyborg, 1965). High streaming velocity gradients in turn result in a large time-independent viscous stress.

In order to avoid dangerous X-ray exposure to the fetus, obstetrics has become the largest area of usage of ultrasound. The fetus in its fluid cavity provides an ideal ultrasonic medium for imaging. It is estimated that 40% of pregnant women in the United States are scanned at least once (Wells, 1984). Because of this routine use, possible biological effects to the fetus are of concern, though it is important to realize at the outset that biological effects do not necessarily imply biological damage.

However, the potential for biological effects must be determined such that the informed physician can make a determination of benefit versus some, as yet unidentified, risk for each patient.

To determine safe levels for ultrasound use during pregnancy, investigators have concentrated on the possibility of mammalian developmental biological effects. Shoji et al. (1972) reported significant increases in fetal mortality and some fetal abnormalities when pregnant mice were irradiated for 5 hours with 40 mW/cm^2, 2.25 MHz ultrasound on the ninth day of gestation. This report has not been verified by other investigators, and a thermal mechanism for damage is suspected (Lele, 1975). Reduction in fetal weight in mice has been shown when pregnant mice were exposed to 1 MHz ultrasound for 5 minutes at an average intensity as low as 1 W/cm^2 (O'Brien, 1976; O'Brien, 1983). These results are most likely strain specific (O'Brien et al., 1982). In extrapolating any animal experimental evidence to the human case, it is important to recognize that, except during the earliest stages of development, <u>in utero</u> exposure to the human fetus does not constitute whole body irradiation as it does in many other animal systems. Proper movement of the transducer and shorter exams limit the exposure of any one area on the human fetus. Time averaged diagnostic intensities are low enough that significant heating of the human fetus is not expected. At the present time there is no direct evidence that diagnostic ultrasound produces any biological effect, harmful or otherwise, on the fetus (Carstensen and Gates, 1984). However, as more sensitive methods for detection of biological damage are developed, we may find that greater damage is occurring than

previously realized. As new clinical applications of ultrasound develop and more patients are exposed to this radiation, it becomes more important to determine all possible biological effects, to identify the physical mechanisms responsible for these effects and to find whether those processes are operative in body tissues.

The objective of this thesis is to discuss the modification, characterization, and implementation of a commercially available ultrasonic scanner to detect ultrasonically induced gas bubble activity, *in vivo*, in the mouse neonate.

The remainder of this thesis is organized as follows. Chapter 2 discusses cavitation phenomena in more detail. The ultrasonic exposure and imaging systems and related hardware used during the irradiation process are discussed in Chapter 3. Chapter 4 describes the experimental procedure employed, and presents and discusses the results of imaging of the mouse neonates during exposure. Chapter 5 presents the conclusions and recommendations for future research.

CHAPTER 2

CAVITATION THEORY

2.1. Cavitation

Acoustic cavitation is a complex, nonlinear physical phenomenon in which the motions of bubbles generated by a sound field bring about typical physical effects (Flynn, 1964). This general definition includes the generation of bubbles by the sound field, the various motions of the bubbles, and the physical effects brought about by these motions. Flynn characterizes bubbles by their motions as either a stable or a transient cavity. Blake (1949) further characterized the transient bubble fields as either gaseous or vaporous. In a gaseous cavity, the relative amounts of vapor and gas remain unchanged during a pulsation. In a vaporous cavity, the vapor-gas composition may change during a pulsation as evaporation and condensation maintain the pressure of the vapor at its equilibrium value.

2.2. Nuclei and Stabilization

Small inhomogeneities, called nuclei, are necessary for cavitation events to occur at moderate sound pressure amplitudes less than the tensile strength of the liquid (Flynn, 1964). Laplace pressures exerted by surface tension cause smaller free bubbles (less than 1 micron) to dissolve, and buoyancy causes larger bubbles to rise to the surface. A 10 micron bubble dissolves in only 7 seconds, while a 1 micron bubble dissolves 1000 times faster, even in gas saturated water. A 100 micron bubble takes 6900 seconds to dissolve, but rises through the liquid with a terminal velocity of 2 cm/sec. To account for the

existence of nuclei in solution, various nuclei stabilization models have been proposed, such as the crevice (Harvey, 1951),the organic skin (Fox and Herzfeld, 1954), the ionic skin (Akulichev, 1966), and the varying permeability skin (Yount, 1979).

The organic skin model proposed a rigid, gas impermeable skin preventing loss by diffusion and giving mechanical strength. Strasberg (1959) found a linear dependence on cavitation threshold with applied static pressure which led Herzfeld (1957) to abandon the model. He reasoned that a crushing pressure should eventually destroy the rigid skin and result in a sharp discontinuity in the cavitation threshold.

Free ions in a liquid can stabilize a pocket of gas by coulomb repulsion (Akulichev, 1966). However, tests of the ionic skin model indicate that the cavitation strength of water is independent of the conductivity due to ions of dissolved substances, even when it is varied by more than two orders of magnitude (Sirotyuk, 1970). This effectively discounted the ionic skin theory. Cavitation threshold, the critical sound pressure amplitude necessary to give rise to cavitation, is influenced by the concentration of the salt KI, but there is not a viable model detailing the physical mechanisms that that lead to nuclei stabilization (Crum, 1985).

The surface active agents model proposed by Sirotyuk (1970) and extended by Yount et al. (1979) is a modification of the organic skin model. Yount's modification led to the varying permeability (VP) model. Surface active molecules provide mechanical compression strength but no tension strength. The skins are effectively impermeable for compressions exceeding

eight atmospheres. Nuclei of widely different radii can be stabilized at the same ambient pressure, and can be cycled and restabilized at different pressures, provided that the threshold for bubble formation is not exceeded (Yount et al., 1984). The nuclei will all have the same internal pressure determined by diffusion equilibrium with the surrounding medium. A detailed review of the model is presented by Atchley (1985). Yount's measurements in supersaturated gelatin indicate that the skins are initially permeable, but become impermeable and stabilize the bubble at a critical radius. So far the model has only been used to predict compression and decompression processes during which diffusion can play a major role.

The most acceptable model for nucleation in water is the crevice model. Gas is trapped in a conical crevice in a solid hydrophobic inhomogeneity present in a liquid. This model can predict many aspects of nucleation. Simple models for gas stabilization in crevices have been considered by several investigators (Harvey et al., 1944; Strasberg, 1959; Flynn, 1964; Apfel, 1970). In these studies, the influence of gas saturation in the liquid, hydrostatic pressure, advancing and receding contact angles, pretreatment of the sample, temperature, frequency and size of the crevice on the cavitation threshold have been investigated.

Various sites of cavitation nuclei have been proposed within biological media. To determine the possibility of cavitation in living tissue, it is critical to know whether nuclei exist and under what conditions they are present. Harvey (1951) found no evidence for nuclei in normal quiescent blood. Using rat

thyrocytes suspensions, Dooley et al. (1983) did not find nuclei which respond to very short pulses. Fulton (1951) found evidence for nuclei generated by muscle activity during decompression studies. Nucleation sites seem to be present in most living organisms including man (Rubissow and Mackay, 1974). Gramiak and Shah (1971) attributed echoes in human cardiac chambers to microscopic bubbles.

The stabilization mechanism in biological media is unknown at this time. Crevices to stabilize gas pockets are probably on the order of tens of microns. The origins of bubbles in the inner ears of monkeys may be the sharp crevices in the bony tissues (Van Liew, 1968; Van Liew and Passke, 1967). For the ionic skin or the VP models to be the stabilization mechanism in tissues, there must be preexisting dissolving gas bubbles. Apparently stabilized gas bubbles less than 1 micron are present in water, but their presence in blood is unknown. From decompression studies, a process called tribonucleation where free gas is introduced by relative movement of tissues is descibed by Hemmingsen (1982). The phenomenon is still not well defined.

A question exists as to whether nuclei of appropriate size exist in tissues (ter Haar et al., 1981, 1982; Crum, 1982; Crum and Hansen, 1982). It will be very difficult to determine the size and distribution of gaseous nuclei in mammalian tissues even assuming their existence can be established, because these quantities are most likely time varying (Carstensen and Flynn, 1982). It has been suggested (Carstensen, 1985) that variability in the presence of cavitation nuclei in subjects could be

responsible for some of the conflicting claims of biological effects from the different laboratories.

2.3. Stable and Transient Cavitation

Bubbles that pulsate over relatively long intervals of time are defined as stable cavities, and bubbles that collapse violently after only a few cycles are defined as transient cavities. The critical pressure amplitude where the transition between stable and transient cavitation occurs is known as the threshold pressure for transient cavitation.

Transient cavitation events can be defined by a variety of criteria. One commonly used criterion is that the velocity of the collapsing cavity approaches the velocity of sound in the medium or that the maximum radius of the pulsating bubble reaches twice the equilibrium radius. Neppiras and Noltingk (1951) show that the velocity criterion is met if the bubble reaches a maximum size of 2.3 times the initial size. Flynn (1964) defines two functions called the inertial acceleration function and the pressure acceleration function to describe cavity motion. A stable cavity is controlled by the pressure function when the maximum radius is less than the critical value. A transient cavity is controlled by the inertial function. Flynn (1982) provides a quantitative basis for the generation of transient cavitation given appropriately sized nuclei. For frequencies in the diagnostic range (1-10 MHz), only nuclei below a few microns (2-3) will grow explosively. The maximum size of nuclei with a well defined threshold decreases as frequency increases.

When a bubble exists in a sound field, the bubble will start to oscillate and act as a secondary source. The scattered and ambient fields are superimposed. The scattered sound pressure near the bubble, p_s, is given by Coakley and Nyborg (1978) as

$$p_s = R_e \quad j\omega\rho_o R_o^2 \dot{\xi}_b / r \tag{2.1}$$

where R_o is the bubble radius, r is the radial distance from the bubble center, and ξ_b is the bubble displacement. The complex amplitude of the scattered pressure is given by

$$\underline{B} = \frac{p_o \Omega^2 R_o}{r} x(\Omega, \delta) e^{j\alpha}$$

$$x(\Omega, \delta) = [(1 - \Omega^2)^2 + \Omega^2 \delta^2]^{-1/2} \tag{2.2}$$

where Ω is the frequency relative to the resonant frequency, δ is the damping constant, and α is the phase angle between p_s and the ambient pressure.

The highly nonlinear oscillations of bubbles in an acoustic field can result at very low pressure amplitudes. When a bubble pulsates, transverse waves are often set up on its surface. At high pressure amplitudes, these surface waves become distorted and unstable. During the collapse of a transient cavity, jets of liquid project into the bubble and microbubbles of air are formed which may serve as new nuclei.

Recently, the potential for transient cavitation from diagnostic ultrasound has been investigated (Flynn, 1982; Apfel, 1982; Apfel, 1986). Flynn reported that violently collapsing

transient cavities produced by microsecond pulses can generate maximum pressures of 1000-7000 bars and temperatures of 1000-20000^{o} K. In comparison, the maximum pressure in stable cavities approaches 100 bars at its minimum radius. Transient cavitation is expected if temporal peak intensities are above thresholds on the order of 10 W/cm^2. Strong shock waves that can result in biological damage can be produced when a bubble collapses. The initial strength of the wave depends on the maximum pressure in the cavity. Apfel (1986) includes viscosity and surface tension effects as well as the inertial effects presented in the earlier calculations (Apfel, 1982). Depending upon carrier frequency and the existence of appropriate nuclei, peak intensities exceeding 2-50 W/cm^2 are required for transient cavitation with microsecond pulses of ultrasound (Carstensen and Gates, 1984).

2.4. Rectified Diffusion

Rectified diffusion is a relatively slow growth process of a pulsating bubble due to an average flow of mass into the bubble over an acoustic cycle. This phenomenon was first suggested by Harvey et al. (1944). Subsequently, a first order theory of a pressure threshold, above which rectified diffusion can occur, was worked out by Blake (1949). Whatever the stabilization mechanism, theoretical cavitation thresholds are usually based on the model of a free nuclei in a liquid. Thresholds depend on such parameters as nuclei size, ambient equilibrium pressure, dissolved air content, temperature, vapor pressure, surface tension, viscosity. frequency, and exposure time, and, if pulsed,

the duty cycle of the sound field. For bubbles of one micron diameter, this threshold exceeds 1 bar (Crum, 1984).

A bubble oscillating about an equilibrium radius can grow in size due to the area effect and the shell effect. The area effect is associated with the increased concentration of gas (moles/l) in the interior of the bubble when it contracts, which causes gas to diffuse from the bubble into the surrounding liquid. Similarly, when the bubble expands, its gas concentration decreases, and gas diffuses into the bubble. Since the diffusion rate is proportional to the surface area of the bubble, more gas will enter during expansion than will leave during the contraction of the bubble. Therefore, over a complete cycle, there will be a net increase in the amount of gas in the bubble.

The diffusion rate of gas in a liquid is proportional to the gradient of the concentration of dissolved gas. The variation in the gas concentration in the liquid adjacent to the bubble, the shell effect, modifies the gas diffusion and must also be considered for an adequate description of rectified diffusion phenomenon (Hsieh and Plesset, 1961; Strasberg, 1961). Bubble growth rates are also influenced by thermodynamic effects (Crum, 1980), inertial effects (Eller and Flynn, 1965), and enhanced by surface oscillations which induce acoustic microstreaming (Gould, 1974).

In conclusion, Crum (1985) defines three possible behaviors of an acoustically stimulated bubble: (i) it can remain unchanged in time-average volume, but pulsate violently, (ii) it can grow explosively in one or two cycles, or (iii) it can grow

slowly by rectified diffusion to a point where (a) it breaks up due to surface wave formation, or (b) it grows explosively as in (ii).

This discussion on the physics of acoustic cavitation is meant as a brief overview. A more complete discussion is presented in review papers by Apfel (1981), Flynn (1964), and Neppiras (1980), and in books by Dunn and O'Brien (1976), and Fry (1978).

2.5. Bioeffects

When the application of sonar resulted in marine deaths, Wood and Loomis (1927) initiated the first extensive bioeffect study. They investigated the killing of small fish and frogs exposed to 300 kHz ultrasound for several minutes, but did not determine the cause of death. A number of physical, chemical and biological phenomena may occur including fragmentation of structures, acceleration of chemical reactions, and damage to biological cells and tissues due to activity set up in or near small gaseous bodies (Coakley and Nyborg, 1978). Over 50 years ago it was shown that the disruptive effects of ultrasound on single cellular organisms are often associated with cavitation (Schmitt and Uhlemeyer, 1930).

The most destructive biological effects associated with stable bubbles are due to the large amplitude oscillations of resonant size bubbles. Usually nuclei must grow to resonant size so pulse length is an important exposure factor. Longer pulses are biologically more effective at a given exposure, yet pulse length must be kept short so that time average intensities are

low enough to rule out heating as a factor in the biological damage.

Much of the work concerning biological effects has concentrated on identifying specific effects and determining threshold levels for selected tissues using various pulsed and continuous wave regimes (Dunn, 1982). Current evidence for the occurrence of cavitation in vivo is based largely on microscopic observations of highly localized tissue damage, which is sometimes attributed to the high temperatures and pressures associated with the unstable collapse of a bubble (ter Haar et al., 1979). Lesions due to very high intensity ultrasound are histologically different from lesions at lesser dosages. Lesions at high intensities are attributed to cavitation activity, while lesser intensities at longer durations result in thermally induced lesions. Several investigators have determined the threshold relationship to produce lesions in the brain to be $It^{1/2}=200$ for single pulse irradiations where I is in W/cm^2 and t is in seconds (Fry et al., 1970; Pond, 1970; Robinson and Lele, 1972). Lele (1977, 1978) irradiated cat brains in vivo at peak intensities of 1500 W/cm^2 in 10 μs pulses (1 kHz repetition rate for 1800 sec) and found no histological damage. Increasing the pulse length to 20 μs resulted in threshold lesions in 20% of the cases. Subharmonic emission, used as an indicator of steady cavitation, had no distinct threshold intensity. Subharmonic emission increased with increasing intensity between 100 W/cm^2 and 1500 W/cm^2 and showed a sharp rise in activity above this level. Anharmonic (wide-band) signals typical of transient cavitation activity had a threshold at 1000 W/cm^2. Histological

damage could be correlated with anharmonic emission above 1500 W/cm^2 with 2.7 MHz ultrasound.

Chan and Frizzell (1977), using 3 MHz ultrasound, found the lesion threshold in liver to be twice that for brain. Differences in the threshold lesions at 550 W/cm^2 and 3000 W/cm^2 suggested a difference in the mechanisms responsible for the damage.

Cavitation is probably responsible for fragmentation and denaturation of DNA in solution by mechanical means (Gooberman, 1960), although chemical effects may also contribute (Alexander and Fox, 1954). The low absorption coefficient of the solution minimizes any thermal mechanism of damage. However, there is disagreement on the levels required to produce effects. Threshold values less than 1 W/cm^2 (Hill et al., 1969; McKee et al., 1977) have been determined, yet damage using 300 W/cm^2 was attributed to noncavitation phenomena (Coakley and Dunn, 1971). The destruction of amoebae has been associated with the specific number of discrete cavitation events (Coakley et al., 1971).

To describe the biological effects of a form of cavitation on Elodea leaves, Miller (1977) invented the new phrase 'gas body activation (GBA).' A reasonable definition of GBA is: the induction and maintenance of oscillation by the interaction of an ultrasonic field with one or more structurally stabilized volumes of gas in a liquid (Miller, 1984). This phrase is now applicable to a variety of situations where preexisting gas bodies seem responsible for the observed effects of ultrasound. Several physical mechanisms for biological effects in the vicinity of activated gas bodies were given by Nyborg et al. (1976). The

biological effects observed were attributed to local heating, large sonically generated radiation forces, acoustic microstreaming at the boundaries, and shear stresses within the cell. Recently developed linear theoretical models for the oscillation of plant-tissue gas bodies (Miller, 1979a) and for gas filled micropores (Miller and Nyborg, 1983) generally agree with experimental evidence.

Elodea leaves were used in one of the first detailed reports of ultrasonic bioeffects (Harvey and Loomis, 1928). Elodea leaves contain naturally occuring gas bodies such that the spatial relationship between the sound beam and the tissue can be determined. Miller (1979b) determined that most gas bodies in Elodea are most strongly activated in the frequency range 3-7 MHz as is predicted by resonance theory. Continuous irradiation for 1 second and pulsed exposure with pulse durations of 1-10 msec resulted in similar thresholds. Cell death threshold (CDT) was about 180-350 mW/cm^2 at 5.25 MHz (Miller, 1979b;Miller, 1983a). For 100 sec cw irradiations at 1 MHz, CDT was approximately 180-500 mW/cm^2, but increased to 2.4 W/cm^2 for 1 sec irradiations (Miller, 1977; Miller, 1979b). Threshold differences were attributed to variations in the size of the gas bodies in the leaves.

Pea roots provide small diameter, highly organized tissue structures for ultrasonic studies. Direct measurement of temperatures in exposed roots indicates that the primary mechanism of action of ultrasound is nonthermal (Eames et al., 1975). Cavitation is the likely mechanism for damage since more damage is seen in the elongating zone of the root (Miller et al.,

1974) where more gas is present (Carstensen et al.. 1981). Irradiation is less effective at frequencies above 2 MHz, under conditions of excess hydrostatic pressure (Carstensen et al., 1979), and for short (30-100 s) pulses (Child et al., 1975) indicating a cavitation mechanism. The threshold intensity for an effect on growth appears to be of the order of 1 W/cm^2, although no simple dose-response relationship is apparent. A complete survey of the effect of ultrasound on plant tissues has been presented by Miller (1983b).

Gas bubbles trapped in nucleopore membranes have produced effects by GBA. Oscillation of the gas bodies probably causes indirect effects through nonthermal mechanisms such as microstreaming and radiation force (Miller, 1984). Bubbles trapped in membranes and included within a suspension of human erythrocytes during exposure to ultrasound resulted in ATP release by lysed cells. Clumping of platelets using a diagnostic Doppler device at low ultrasonic intensities can be observed (Miller et al., 1978). Continuous wave exposure of 1.6 MHz at spatial peak intensities of 20-30 mW/cm^2 using 4 m diameter pores resulted in ATP release (Williams and Miller, 1980). Results for pulsed mode exposures with 1-100 s pulses and a 1:10 duty factor are comparable to continuous exposures with the same SPTA intensity without regard for variations in pulse duration (Miller and Williams, 1983). The frequency or magnitude of clumping of platelets and cell lysis <u>in vivo</u> at diagnostic frequencies would most likely be below the natural occurrence of these processes, and would would be accommodated by the body's homeostatic processes (Carstensen, 1985).

Fruit flies may provide the needed bridge between plant and animal studies (Child et al., 1980). Drosophila larvae provide a good animal model for GBA, since gas bodies of less than 1 micron, which can serve as transient cavitation nuclei, are stabilized in the tubules of their respiratory apparatus just prior to hatching. Diffusion from the highly absorptive eggs prevents large increases in temperature at the lethal exposures. The frequency dependence of absorption suggests either a wide distribution of bubble sizes and resonant frequencies (Carstensen et al., 1983) or an aggregate response of closely packed channels (Miller, 1980). Sensitivity to the pulsed ultrasound increases markedly after air is taken into the respiratory system (Child and Carstensen, 1982). Microsecond pulses of 2 MHz ultrasound of spatial peak temporal peak (SPTP) intensities of 10-20 W/cm^2 for 30 seconds resulted in death. Temporal average intensities in diagnostic ultrasound are one to three orders of magnitude smaller than this value. Decreased survival rates were observed for spatial average temporal average (SATA) intensities of 3 mW/cm^2, indicating the importance of peak intensities in determining possible biological effects and average intensities as an indicator of tissue heating (Child et al., 1981). The killing of larvae using microsecond pulses of ultrasound showed a frequency dependence consistent with a transient cavitation mechanism (Berg et al., 1983). Continuous wave ultrasonic intensity levels of 1 W/cm^2 are required to produce observable biological effects (Fritz-Niggli and Boni, 1950; Selman and Counce, 1953; Counce and Selman, 1955; Pay et al., 1978; Child et al., 1980). For 30 second 1 MHz cw exposures, intensities

above 2 W/cm^2 resulted in progressively greater likelihood of death (Carstensen and Child, 1980). Thresholds for effects of cw ultrasound on Drosophila and plant roots are both in the range of 1-2 W/cm^2. Pulsed exposures in Elodea and Drosophila show similar dependence on temporal peak intensities for the observed biological effects.

Though model studies including insects and plant tissues are vital in developing an understanding of cavitation phenomena, in vivo studies involving mammals are necessary to determine possible biological effects of ultrasonic exposure to humans. Using a commercial therapy unit with a focused 0.75 MHz transducer, ter Haar and Daniels (1981) reported that acoustic cavitation, leading to stable bubble production, occurs in vivo in mammalian tissue as a result of irradiation with ultrasound above 80 mW/cm^2 spatial average intensity in the leg of a pig. They detected bubbles using an imaging system which was capable of detecting gas bubbles with diameters greater than or equal to ten microns, although no accurate measurements of bubble diameter could be made (Daniels et al., 1979). Signals derived from multiple bubbles whose separation was less than the resolution of the system could not be differentiated from those from single scattering centers of the same cross section. The observed production of stable cavitation bubbles in tissues, at the frequency and intensities used by ter Haar and Daniels, can be predicted on the basis of currently available theory concerning the growth of bubbles by rectified diffusion (Beck et al., 1978). Under the specific experimental conditions, Crum and Hansen (1982) conclude that cavitation nuclei would grow above the four

micron resonance size by rectified diffusion to sizes great enough to be observed. During decompression studies using the system, two types of events were defined (Daniels et al., 1980). Single frame events are believed to represent intravascular bubbles passing through the plane of the scan. Persistent events, echoes recorded on two or more consecutive frames, may represent either intra- or extravascular gas bubbles. In studies not involving decompression, no clear distinction between single frame and persistent events can be made. Possibly a single frame event may represent an extravascular bubble oscillating in size about the detection threshold of the recording system. The bubbles are probably largely extravascular, since ECG recordings did not show modifications usually associated with intravascular bubbles (ter Haar and Daniels, 1981). The number of sites of appearance and number of new echoes are proportional to the intensity and time of irradiation with the 0.75 MHz ultrasound.

In 1982, ter Haar et al. suggested multiple sites for cavitation with each having a different activation energy. Events observed at and below 300 mW/cm^2 were predominantly on the incident side of the leg and associated with tissue interfaces and subcutaneous fat. At the highest intensity used, 680 mW/cm^2, sites occurred throughout the entire cross section, with many located intramuscularly. The proportion of single frame events decreased at the highest intensity level.

In pioneer studies conducted in this laboratory on the effects of high intensity ultrasound on nervous tissue, Fry et al. (1951) concluded that hind limb paralysis of frogs was not due to cavitation. Their study broadened to include mammalian

systems, specifically the mouse neonate, where they continued to use a functional, rather than a histological, endpoint for biologic effect (Dunn, 1956; Dunn and Fry, 1957). The third lumbar region, containing a rich supply of motor neurons, resulted in hind limb paralysis at sufficient ultrasonic doses. The neonates provide almost an ideal animal preparation, because they are small, poikilothermic animals, capable of large temperature changes without adverse effect, which have yet to undergo complete ossification of the spinal column. Threshold levels for paralysis of mice was approximately one eighth of that for human brain (Dunn, 1958; Dunn and Fry, 1971).

More recently, Frizzell et al. (1983) determined the exposure conditions for 10%, 50%, and 90% reversible hind limb paralysis at 1 MHz, 10° C, and 1 and 16 atm exposures for the intensity range 86-289 W/cm^2. A shift in the threshold and a decrease in half-harmonic emission were reported to occur at the highest intensity level when excess hydrostatic pressure was applied. The threshold was virtually unchanged with pressurization for intensities at and below 144 W/cm^2.

Various cavitation detection schemes were employed throughout the course of the neonate exposure project including sub- and superharmonic detection (Aschenbach, 1982). An ultrasonic pulse echo bubble detector consisting of an oscilloscope, pulser-receiver electronics, and an imaging transducer was developed (Morimoto, 1984). Transducers of either 10 or 15 MHz center frequency were used to produce A-scans within the spinal cord of the neonate. This scanning technique will

be discussed in a later chapter. The most recent method to detect *in vivo* cavitation activity utilizes a commercial opthalmic scanner.

CHAPTER 3

ULTRASONIC IRRADIATION AND IMAGING SYSTEMS

3.1. Ultrasonic Irradiation System

A block diagram of the irradiation system is given in Fig. 1. An unfocused 3.18 cm diameter X-cut quartz disk resonant at 1 MHz generates the ultrasonic field. The source is mounted at one end of a cylindrical stainless steel chamber housed in a deep freeze unit. The unit is filled with propylene glycol and equipped with heating and refrigeration elements to allow for irradiations at various temperatures. The temperature of the glycol is maintained a few degrees below the irradiation temperature and a YSI proportional controller with a thermistor sensor controls a 300 W heating element within the chamber to regulate the temperature of the degassed Ringer's acoustical coupling solution. Opposite the transducer is a large volume of highly absorbing castor oil. The presence of oil, held by a thin rubber retaining wall mounted at 45 degrees, assures that the neonate is exposed to essentially a travelling wave field. A coordinate system with three orthogonal axes provides an accurate positioning system for the mouse neonate within the sound field. The chamber can be sealed and pressurized up to 20 atmospheres.

The 1 MHz RF signal is generated by a Wavetek model 3006 signal generator, then gated using a minilabs SRA1-H RF mixer controlled by a CMC model 786C dual preset counter, and amplified by an ENI A-500 RF power amplifier. The counter can be programmed for the desired duration, and the amplifier is capable of generating 500 W over the frequency range of 0.3-35 MHz. An

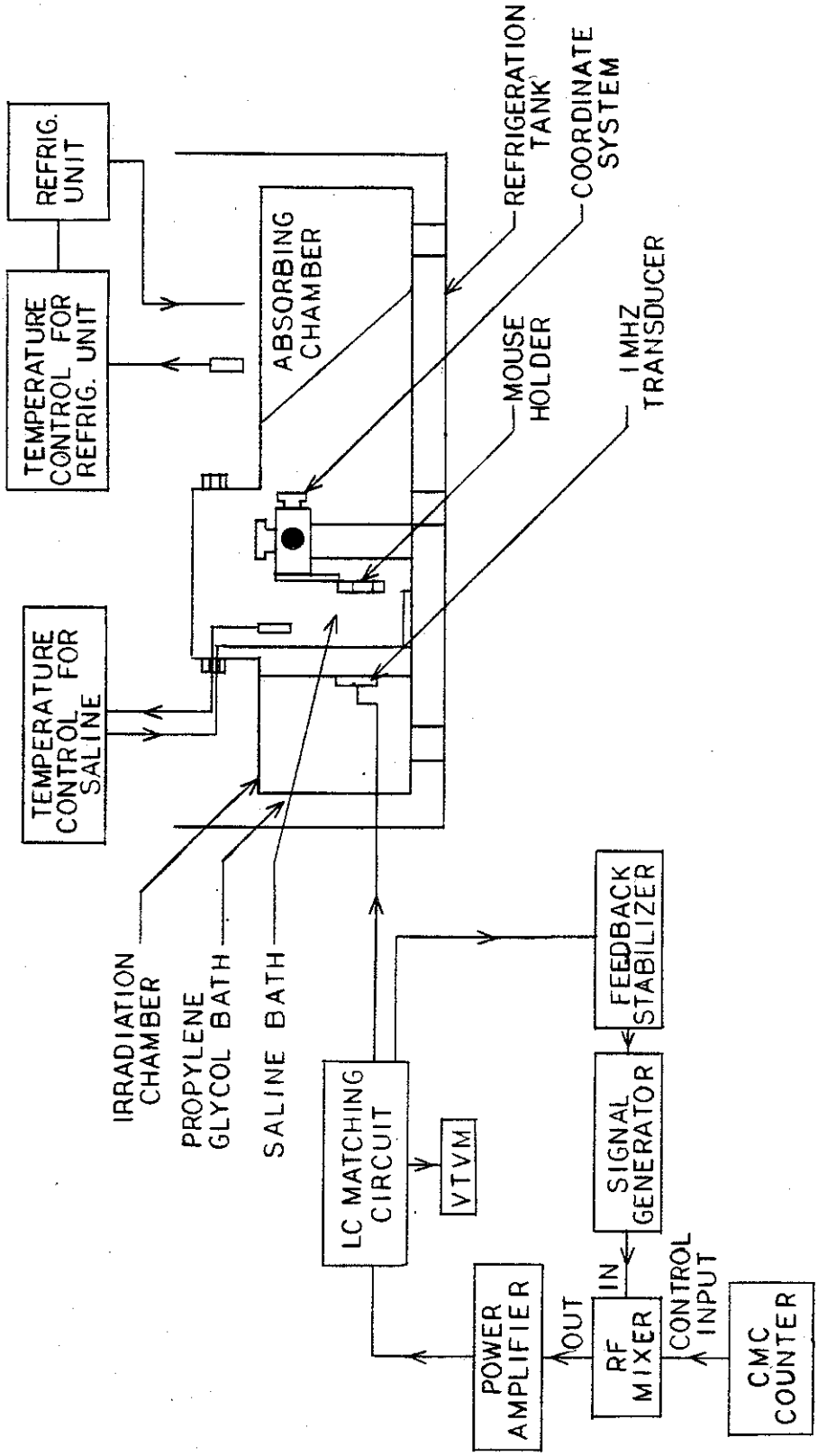

Figure 1. Block diagram of the neonatal mouse irradiation system.

LC matching network between the amplifier and the transducer, and the stabilizing network which assures a constant ultrasonic intensity are described in detail elsewhere (Lee, 1982).

The transient response of a thermocouple embedded in absorbing oil and calibrated against a suspended steel ball radiometer is used to calibrate the ultrasonic field. A complete description of the calibration technique is given in Lee (1982).

3.2. Ultrasonic Imaging System

A commercial opthalmic scanner (Ocuscan 400, Sonometrics Inc.) equipped with a 10 MHz ceramic transducer is used to detect bubbles *in vivo* (Fig. 2). Visualization of internal body tissues and structures in Amplitude-mode (A-mode) operation involves sending short pulses of ultrasound into the body and using the amplitude, direction, and arrival time of reflections received from various tissues with different acoustic impedance (the product of density and velocity within the tissue) to produce a real time image. Ultrasonic pulse echo imaging utilizes signals typically in the 1-10 MHz range generated by a piezoelectric transducer which converts an applied electrical pulse signal into an acoustic pulse of a few cycles. Received reflections are converted into voltage pulses by the same transducer acting as a receiver. The amplitude of the displayed signal is determined by the amplification, compensation, compression, and rejection of the receiver. Emitted pulses are scanned across a plane in Brightness-mode (B-mode) operation and echoes are displayed in two dimensions to produce a bistable (on or off) cross sectional image. A biometry unit. included with the scanner, determines

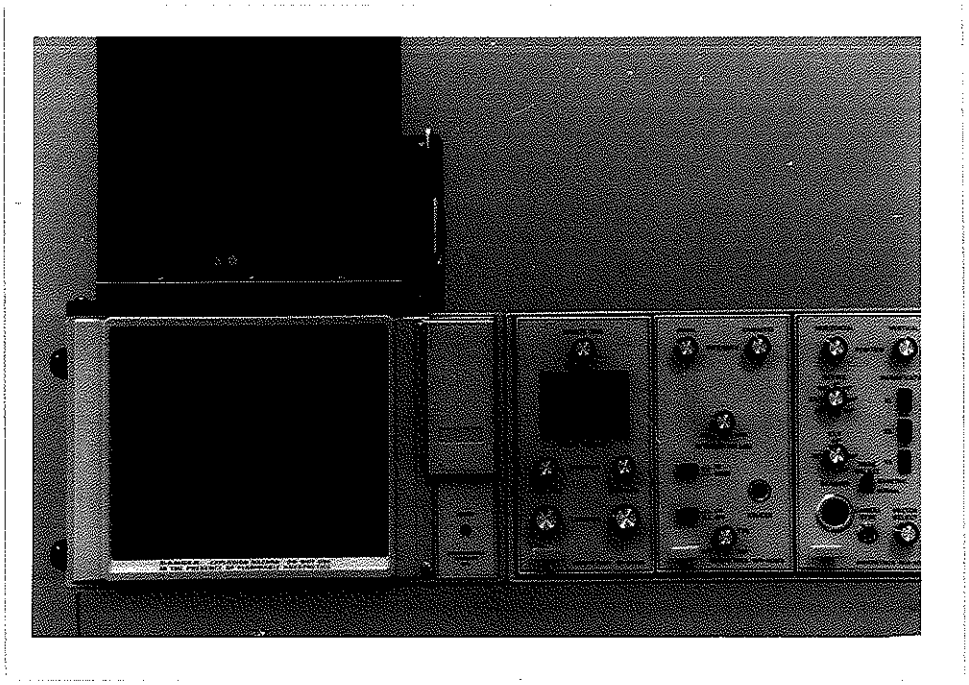

Figure 2. Commercial scanner used to image neonatal mice.

the distance between any two chosen reflections above a minimum amplitude when programmed with the ultrasonic speed in the tissue. The distance along the line of sight of the transducer is calculated from the arrival time of the reflections and then diplayed on the screen. The position of the line of sight must be correctly identified to assure that the correct distance is being measured. Since different tissues have different velocities, the distances are only approximate for nonhomogeneous samples. All calculations and biometry measurements assume an average tissue velocity of 1540 m/s.

The imaging transducer (Fig. 3), modified for submergence (Fig. 4), has a 3.5 cm focal length and a 4 mm diameter. Since stronger focusing provides a very fine resolution over a small range near the focal point, and weaker focusing provides a somewhat coarser resolution over a broader range, the focal point of the transducer is chosen to provide good resolution over a moderate range.

The focal volume of the transducer is determined from the transverse diameter and the axial length of the field at the focal region (Fig. 5). For a focused transducer, beam width at the focus depends on the aperture and the focal length. The half power transverse diameter (D_t) which is the distance across the focal region perpendicular to the direction of propagation where the intensity is reduced to one-half the peak value, can be approximated as,

$$D_t = k_t \frac{F\lambda}{D} \qquad (3.1)$$

Figure 3. Imaging transducer.

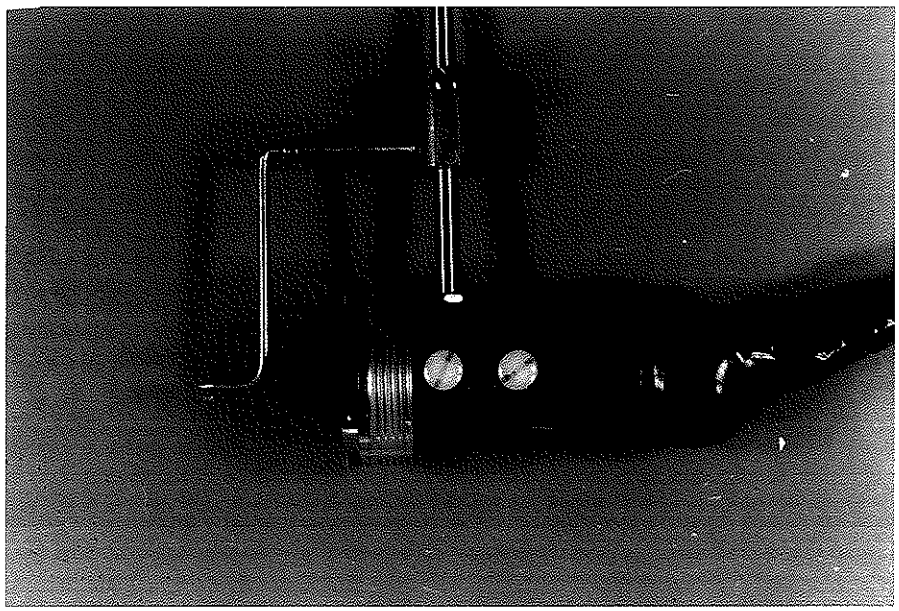

Figure 4. Modified imaging transducer unit.

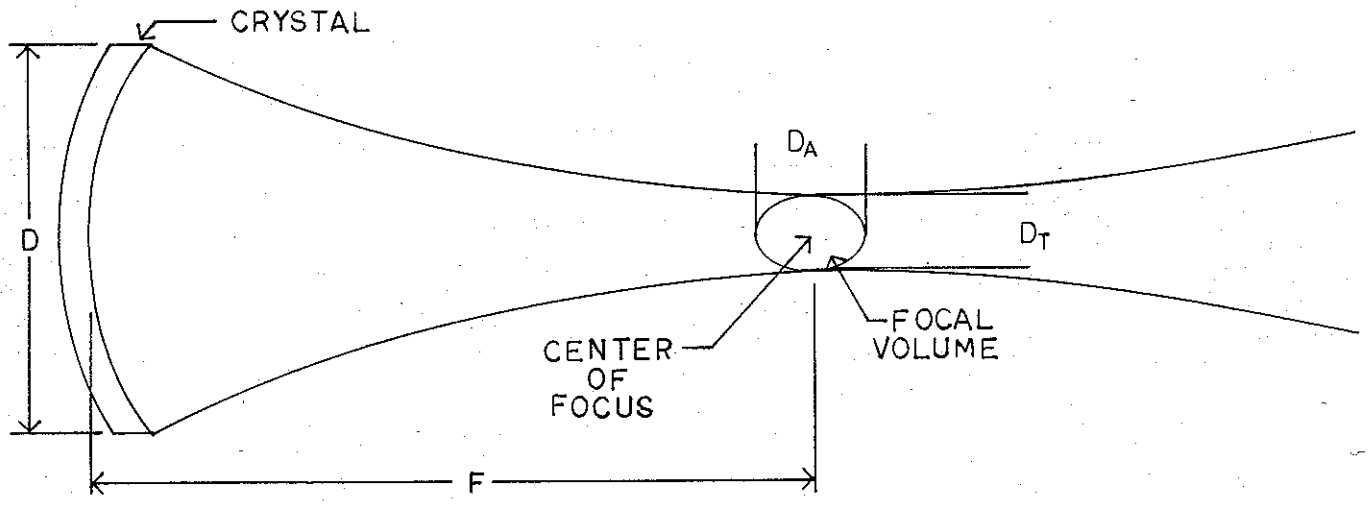

Figure 5. Parameters describing the half power dimensions of the focal volume.

where F is the focal length, λ is the wavelength in the medium, D is the diameter of the transducer, and k_t is dependent on the half aperture angle. To permit calculation within 20% accuracy, k_t can be taken to have a value of one (Fry and Dunn, 1962). The axial length of the focus (D_a) is approximated as

$$D_a = k_a D_t \tag{3.2}$$

where k_a is dependent on the half aperture angle (ψ) (Fry and Dunn, 1962).

The beam profile was determined using a pulse echo (A-mode) technique and a needle reflector (Fig. 6) mounted in a tank attached to an automated millbase capable of movement in three directions. The needle was specially constructed with tapers of 45 degrees to minimize reflections from those interfaces. A B-scan of the needle at 2X magnification is given in Fig. 7. The transducer focus, measured from the front plane of the transducer to the focal point, is reported to be 3.5 cm. However, with the membrane attached to the nosepiece surrounding the transducer, the working range of the unit is confined between the membrane and the focal point. The A-scan was displayed on an oscilliscope, and the peak voltage amplitude of the received reflection from the needle, relative to the baseline, was recorded. The voltage amplitude was attenuated (30 dB) to avoid saturation of the signal at the focal point. Starting at the membrane of the stationary transducer, the needle was scanned in the axial direction to determine the focal distance. The needle was then moved along the vertical and horizontal directions in

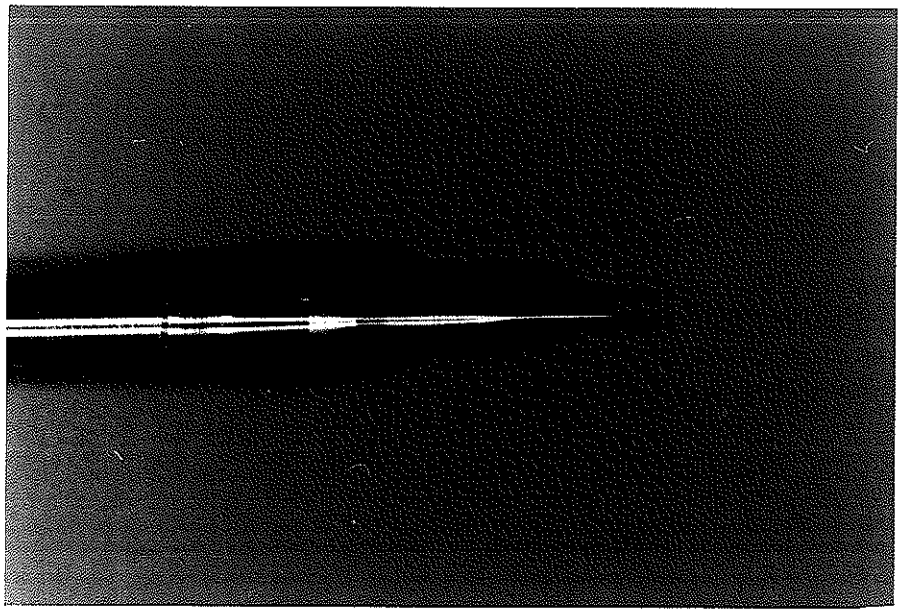

Figure 6. Needle used to plot the beam profile of the imaging transducer.

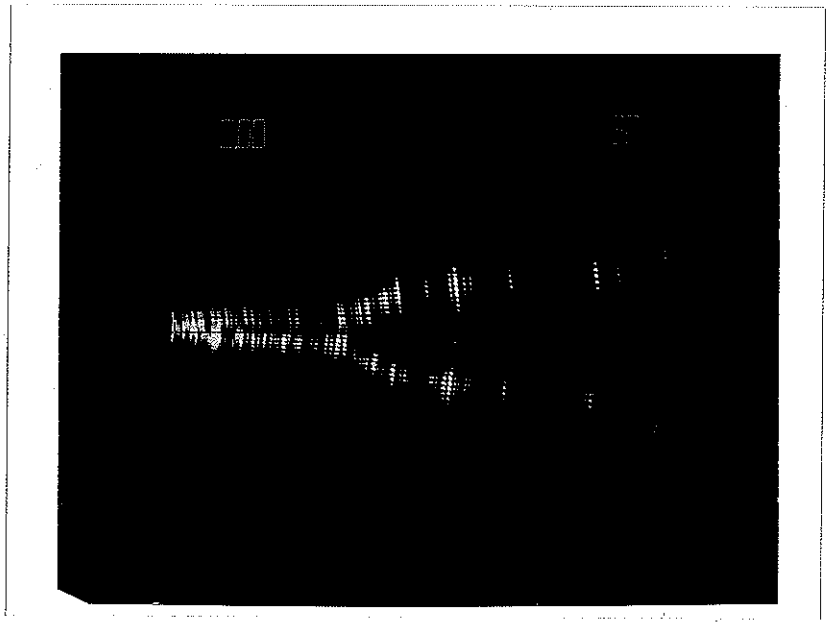

Figure 7. Ultrasonic image of needle.

the focal plane and the results plotted. The working range and the 95% beamwidth at this distance was determined to be 2.65 and 0.34 mm, respectively. The nosepiece of the transducer unit which was designed so that water could be placed inside and used as a coupling medium, was not necessary when the unit was submerged. The beamwidth of the transducer was not affected by the removal of the membrane, but the amplitude of the received signal increased due to decreases in attenuation and reflection from the membrane during transmission and reception. The focal distance was found to be 2.5 cm, which is shorter than reported by the manufacturer. The 3 dB beamwidth, which corresponds to the 6 dB beamwidth when pulse echo techniques are used, was determined to be 1.1 mm in the focal plane. Using the experimentally determined focal length and letting D_t equal 1.1 mm, Equation 3.1 indicates that the operating frequency of the transducer may be below that reported by the manufacturer.

Pulsed ultrasound is characterized by the exposure parameters of pulse duration (PD), pulse repetition frequency (PRF), or pulse repetition period (PRP), and the examination period (Fig. 8). The imaging system used in this study had parameters of

$$\begin{aligned} PD &= \frac{5 \text{ cycles}}{10^7 \text{ cycles/sec}} = 0.5 \ \mu\text{sec} \\ PRF &\simeq 1880 \text{ Hz} \\ PRP &\simeq 0.56 \text{ msec} \end{aligned} \tag{3.3}$$

and a duty factor less than 1/1000. Transducers are designed to optimize resolution by limiting the pulse duration while

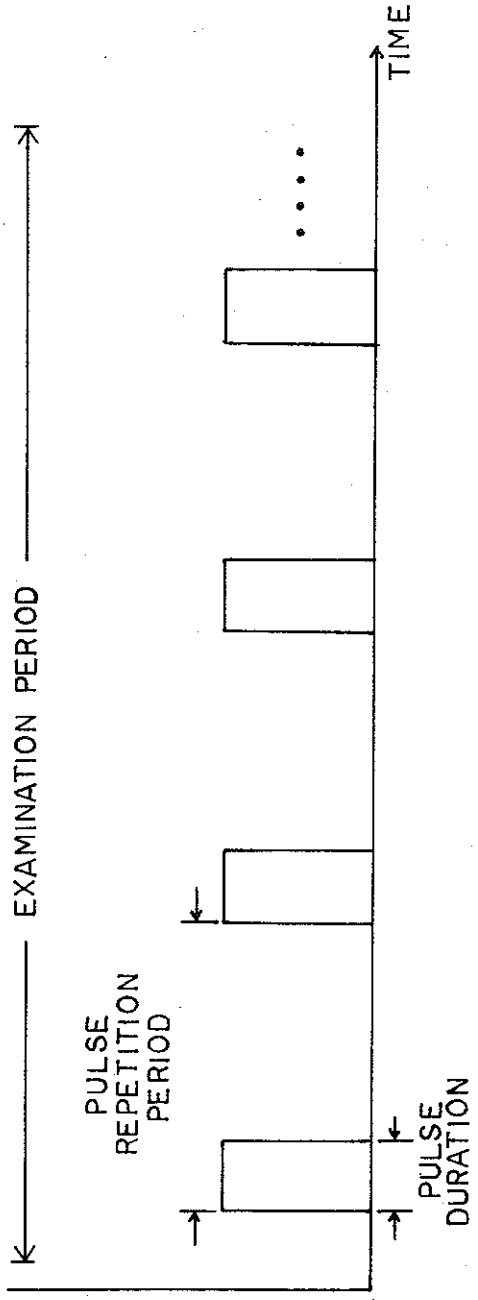

Figure 8. Exposure parameters for pulsed ultrasound.

maintaining adequate sensitivity.

Lateral resolution is defined by the lateral extent of the focal region and axial resolution by the spatial pulse length. The resolution cell of the transducer is roughly an ellipsoid of revolution. Axial resolution is normally better than lateral resolution in diagnostic units so that the major axis is in the transverse direction. Axial resolution (along the direction of sound travel) determines the minimum separation between reflectors along the direction of propagation that will produce separate echoes. Bubbles separated by less than half the spatial pulse length (SPL) are not resolved (Fig. 9), but bubbles separated by more than half the SPL are resolved (Fig. 10). The 3 dB axial resolution is given by

$$\begin{aligned}\text{Axial Resolution} &= \frac{1}{2}\,\text{SPL} = \frac{1}{2}(5\ \text{cycles/pulse})(0.15\ \text{mm/cycle}) \\ &= 0.375\ \text{mm}\end{aligned} \tag{3.4}$$

Lateral resolution is the minimum separation, in the direction perpendicular to the direction of propagation, between two reflectors such that when the beam is scanned across them two separate reflections are produced. If lateral separation is greater than the beam diameter, two separate reflections are produced (Fig. 11). The axial and lateral resolutions define the lower limit on separation between bubbles if they are to be observed individually. A group of bubbles would be observed as a single bubble with a diameter equivalent to the combined cross sections plus the spacing if the bubbles were within the minimum separation.

Mechanical scanning by rotating the transducer back and

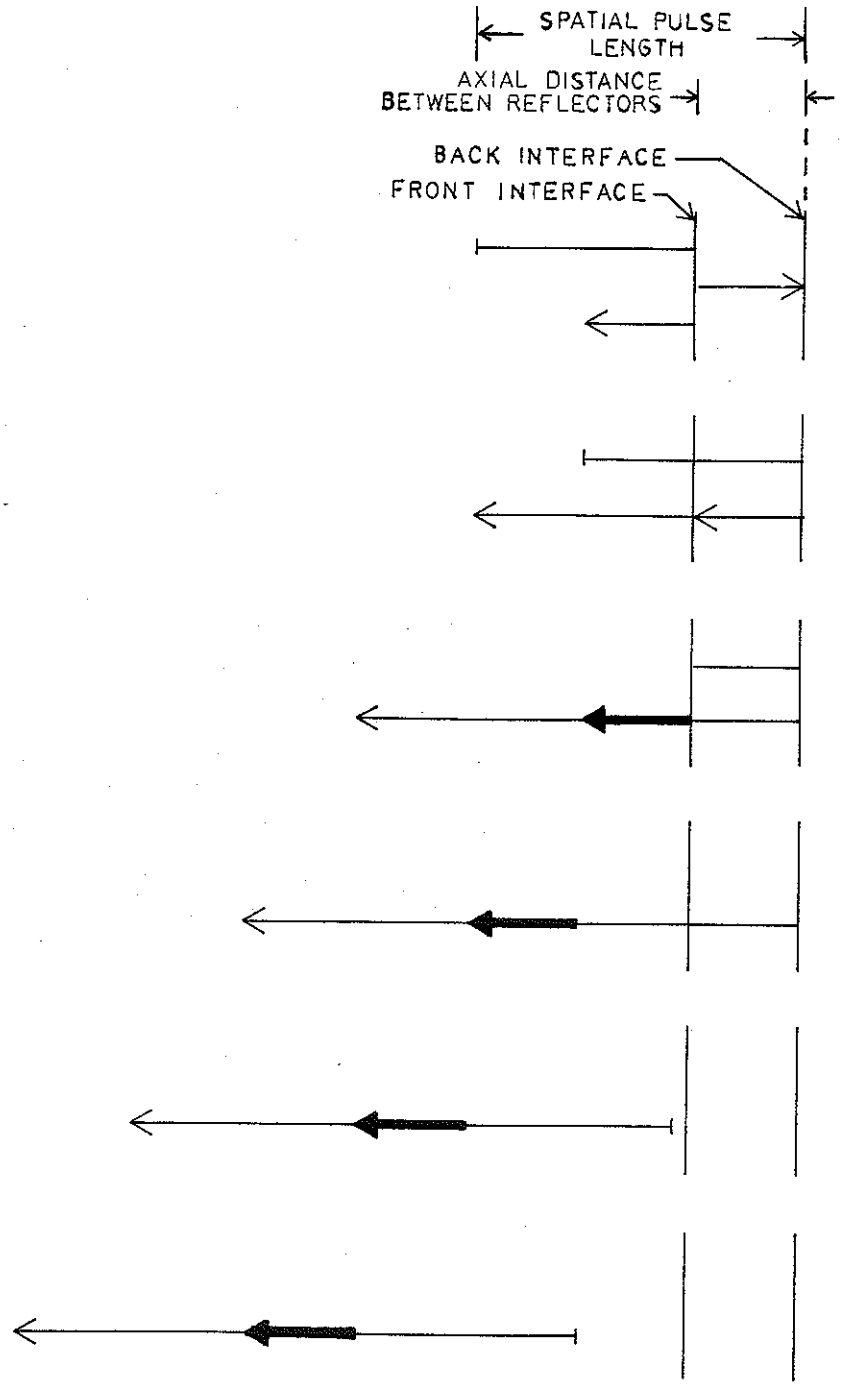

Figure 9. Reflectors with axial separation less than half the spatial pulse length are not resolved (Kremkau).

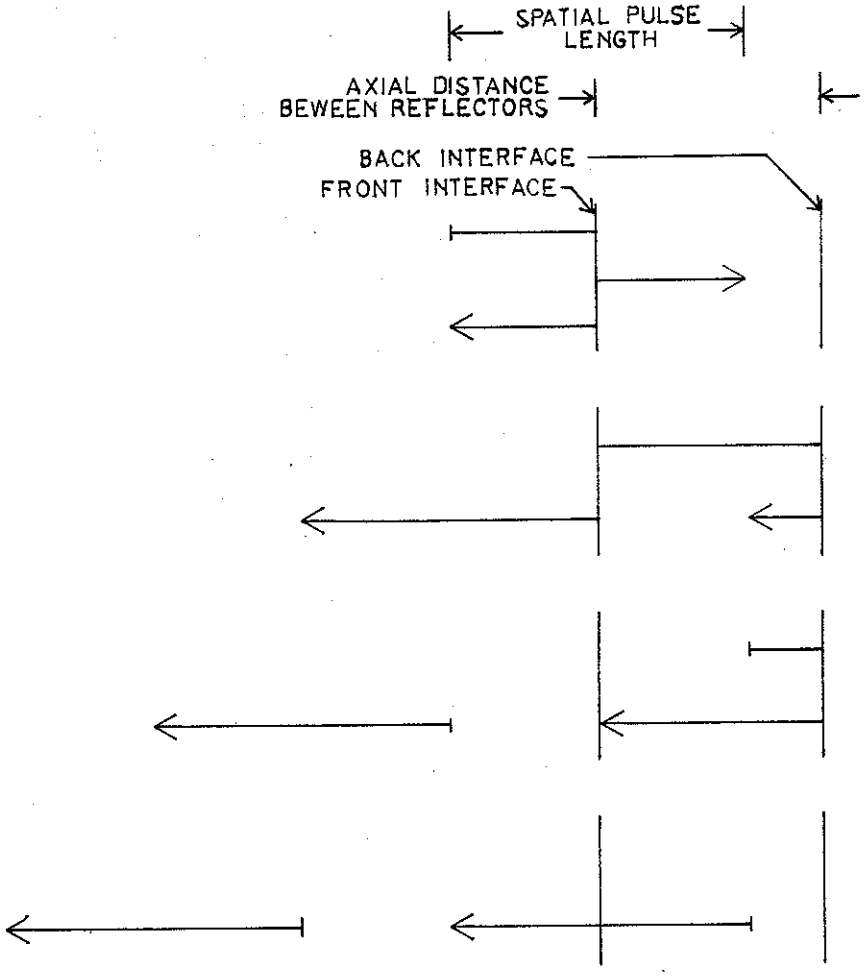

Figure 10. Reflectors with axial separation greater than half the spatial pulse length are resolved (Kremkau).

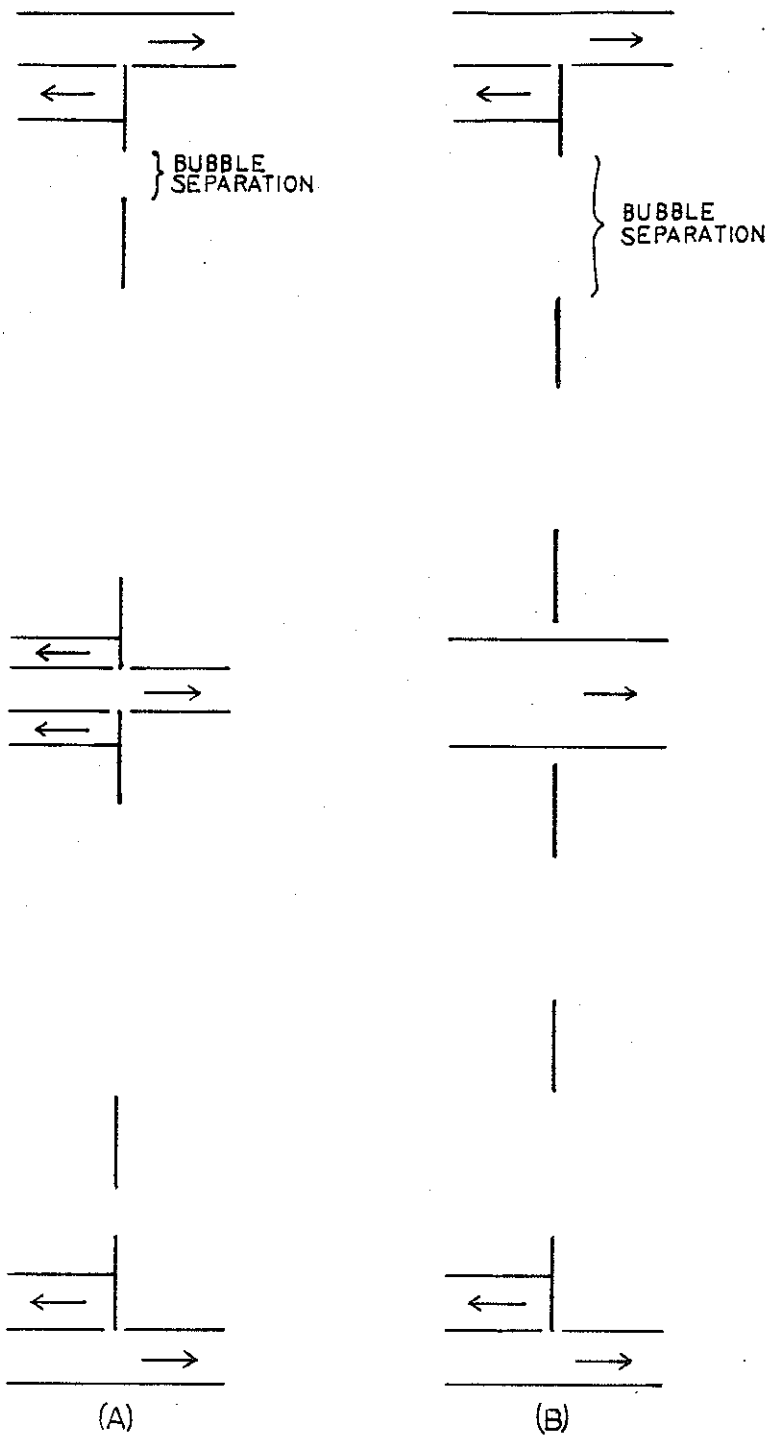

Figure 11. Lateral bubble separation less than (A) and greater than (B) beam diameter results in resolved and unresolved bubbles respectively (Kremkau).

forth through a sector angle produces rapid, repeatable, and sequential scanning of the beam through the object. The real time capability of the scanner allows for two-dimensional imaging of the motion of moving structures. Real time processing requires a high frame rate (FR) and line density (LD) to produce a flicker free, high density image. A frame is the displayed image produced by one complete scan of the sound beam through the 37^{o} sector angle. Each frame is composed of many scan lines (one for each time the transducer is pulsed). The 97 scan lines and the sector angle for this unit are visible when the brightness is increased sufficiently (Fig. 12).

The use of a real time B-scanner for detection of cavitation activity has several advantages over subharmonic monitoring. The imaging system helps to identify the anatomical sites of the onset of cavitation and possibly the sites of cavitation nuclei. Any movement of the neonate due to radiation forces as a result of the 1 MHz ultrasound can be observed. This movement may force the neonate out of the focal region and thereby decrease lateral resolution, unless the position of the scanner can be changed to compensate for this movement as suggested by Morimoto (1984).

Problems have been encountered using the imaging system. Nonlinear propagation of the 1 MHz irradiation wave and the resulting generation of harmonics is a problem when the broadband 10 MHz imaging transducer is operating simultaneously. Harmonics of the wave decrease in amplitude with frequency, but increase with intensity. The frequency spectrum at various intensities from a metal cylinder, used to emulate the spinal cord, was examined by Morimoto (1984). It is clear that although the

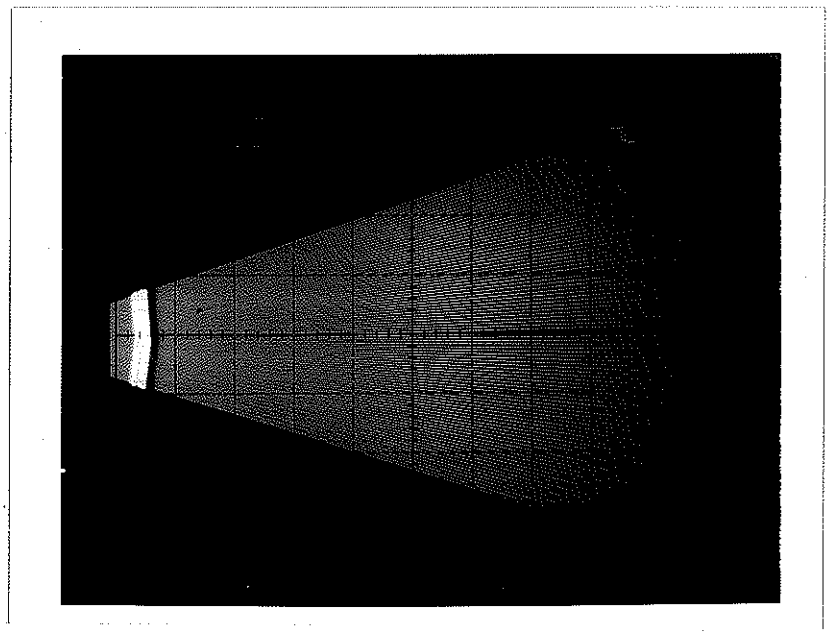

Figure 12. A B-scan image showing scan lines and sector angle.

imaging transducer has a frequency response centered around 10 MHz, the harmonic generation at the high intensities used in this study are significant at 10 MHz and higher. Decreasing the bandwidth by using a bandpass filter to eliminate harmonics other than 10 MHz would result in increased ringing and decreased resolution. Highpass filtering can be effective at lower intensities where higher harmonics do not contribute appreciably to the noise spectrum but is largely ineffective at the intensities necessary to observe cavitation (above 144 W/cm^2). Thus, interference from the harmonics associated with the irradiation beam continues to be a problem.

Since the transducer assembly was designed for ocular scanning, the use of the 10 MHz scanner is limited to atmospheric pressure.

The two main types of artifacts in pulse echo imaging are a result of lateral and axial resolution properties. The finite beam width tends to elongate targets transverse to the beam so that a point target appears as a line perpedicular to the beam axis. This phenomenon is evident in the B-scan of the needle reflector (Fig. 7). Reverberation (multiple reflection) is another common artifact which appears when large impedance mismatches are present. For two internal interfaces, apparent reflectors appear on the display behind the second real reflector at separation intervals equal to the separation between the first and the second real reflectors (Fig. 13). Reverberation from the front surface of an object to be imaged, although common, is easily identified and can be minimized by use of impendance matching.

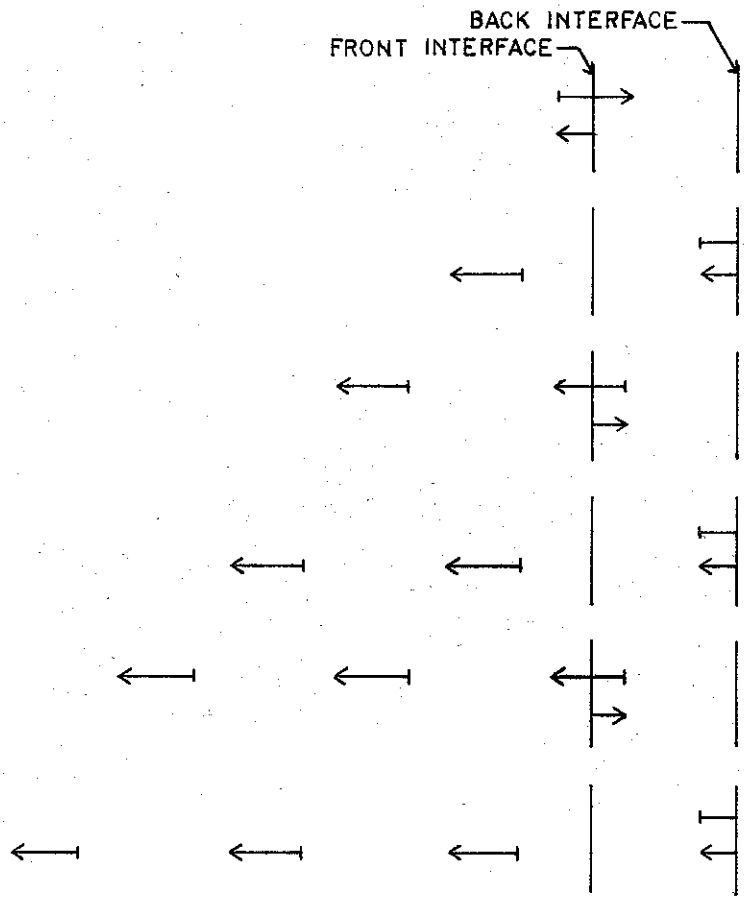

Figure 13. Reveberation from two reflectors (Kremkau).

3.3. Acoustic Detection in vivo

Pulse echo imaging, and specifically the imaging of bubbles in vivo, relies on the part of the scattered field that is reflected back toward the transducer to produce an image. The backscattered intensity varies with frequency and scatterer size. Specular reflections occur when the interface is large compared to the sound beam. An extended interface between air ($z=4x10^3$ kg/sec m^2) and water ($z=1.53x10^6$ kg/sec m^2) will reflect about 99.9% of the incident sound. If boundary dimensions are comparable to or small compared to the wavelength, or the boundary is not smooth, the incident sound is scattered. In general, intensities backscattered from a single scatterer are much less than those from a specular reflector. Scattered intensity decreases as reflector size, relative to the incident wavelength, decreases. However, a bubble with a circumference less than twice the wavelength of incident sound is a much more effective scatterer than a similar size rigid sphere (Fig. 14). For 10 MHz ultrasound, this size corresponds to any bubble less than 4.9 microns in tissue. Scattering from bubbles this small is relatively independent of the direction of the incident sound and is, therefore, more characteristic of the scatterers. Although the 10 MHz signal has a half intensity depth of approximately 3mm in soft tissue and is reduced by 90% in 1 cm, imaging within the shallow depth surrounding the spinal cord of the neonate does not present a problem.

The detection of bubbles and the determination of their size in vivo present some special problems. Doppler techniques to identify moving bubbles have been used extensively in the study

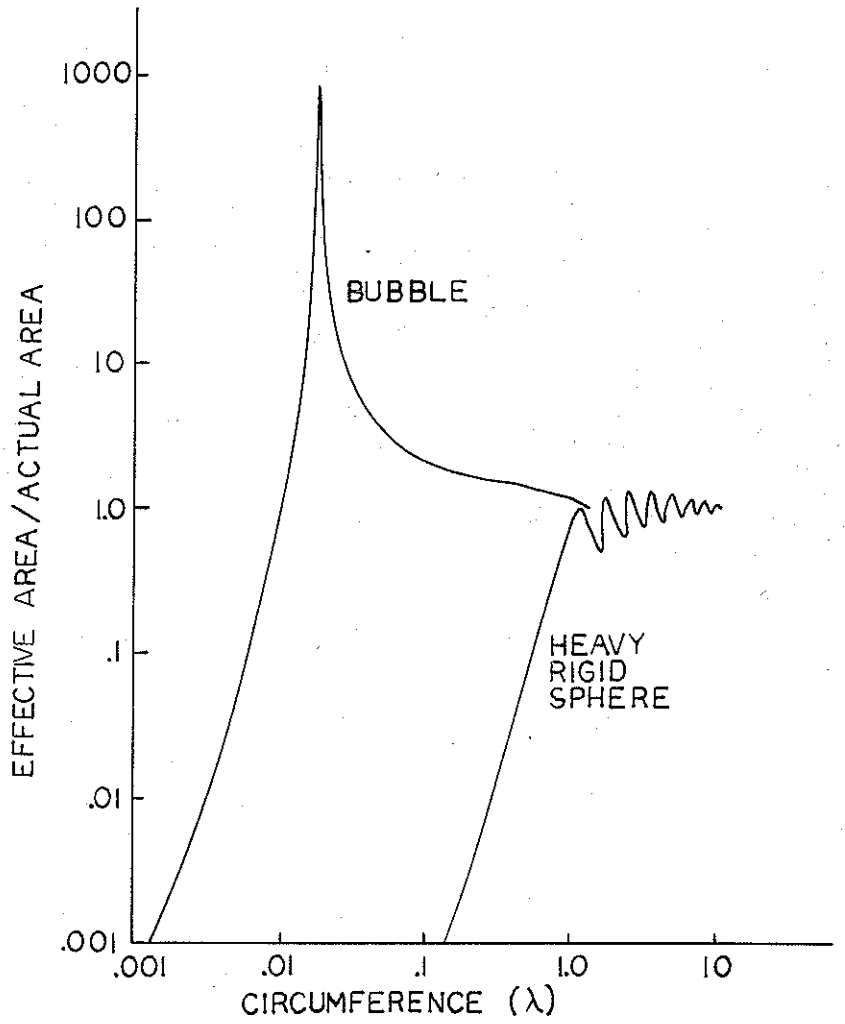

Figure 14. Scattering by a bubble and a rigid sphere (Mackay and Rubissow).

of bubble formation in decompression sickness. However, stationary bubbles could not be detected, so that other imaging techniques have been developed. Chapelon et al. (1985) insonified bubbles simultaneously with a "pumping field," which is swept through the resonant frequencies, and an "imaging field" having spatial resolution to ultrasonically estimate the size distribution of bubbles in the fluid. A similar technique uses multiple frequencies to determine the frequency of maximal scattering. Maximal scattering will occur at the resonant frequency where the scattering cross section may be ten times the geometric cross section. For bubbles much larger than resonance, the cross section approaches the actual cross section. The resonant frequency of a gas bubble in a liquid increases as the bubble size decreases and the hydrostatic pressure increases. The expressions for the resonant frequency and the scattering cross section in water for frequencies of 1 MHz or higher as given by Coakley and Nyborg (1978) are

$$\omega_o^2 = \frac{3\gamma p_o'}{\rho_o R_o^2}$$

$$\sigma_s = \frac{291}{\delta} \pi R_o^2 \qquad (3.5)$$

$$p_o' = p_o\left(1 + \frac{2\sigma(3\gamma - 1)}{3\gamma R_o p_o}\right)$$

where γ is the ratio of specific heat, P_o is the static pressure, σ is the gas-liquid surface tension, and R_o is the resonant radius. The resonant radius at 1 MHz was found experimentally to be 3.5 microns, which corresponds to γ=1.2.

The complex amplitude of the scattered pressure, $\underline{B}$, at the surface from a resonant 3.5 micron bubble in fresh water when irradiated by a 10 MHz signal with a SATA intensity of 0.2 mW/cm^2, a SP/SA ratio of 13 (determined roughly as the area of the transducer divided by the half power area of the focal region), a damping constant of 0.145, and a duty factor of 1/1000 is

$$SPTP = \frac{SATA(SP/SA)}{\text{duty factor}} = 2600\ mW/cm^2 = \frac{1}{2}\frac{p^2}{\rho_o c}$$

$$P = 195\ kPa = 1950(10^3)\ dynes/cm^2$$

$$\underline{B} = p\Omega^2 \frac{R_o}{r} x(\Omega,\delta)e^{j\alpha} = 1970(10^3)e^{j\alpha} \qquad (3.6)$$

$$x(\Omega,\delta) = 0.0101$$

$$\alpha = -0.014 \text{ radians}$$

This scattered pressure is not much greater than the incident pressure, since the irradiation frequency is ten times the resonant frequency of the bubble. The very large resonant peak of the scattered signal from a bubble in water may be highly damped in a biological fluid so that monitoring several frequencies for maximal scattering may be ineffective for determining size <u>in vivo</u>. The response falls off rapidly, as r^4, where r is the radius of the bubble, so there is little prospect of detecting bubbles smaller than resonance size (Evans, 1977). The dependence of scattered intensity (normalized by the incident intensity) at 1 cm from the bubble on frequency is shown in Fig. 15.

Since first suggested by Mackay (1963), the implementation and characterization of a pulse echo imaging system for the study

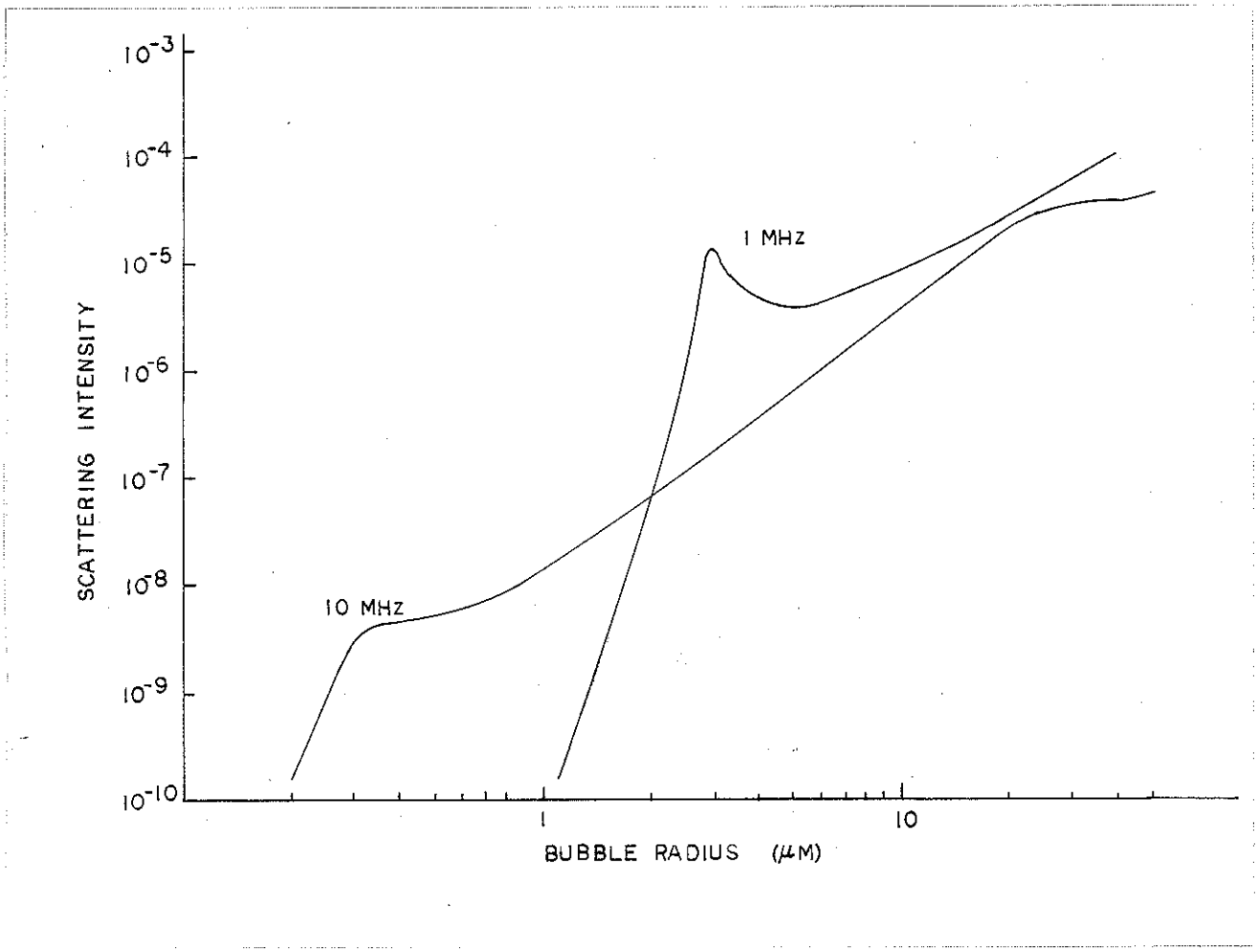

Figure 15. Scattering as a function of bubble size at 1 and 10 MHz (Nishi).

of bubbles has met with skepticism. Rubissow and Mackay (1974) reported that pulse echo ultrasound of wavelength 200 microns could detect bubbles as small as 0.5 microns. Evans (1977) and Nishi (1977) challenged this claim. The smallest single bubble detected by Hills and Grulke (1975) were 150 microns in diameter. Nishi argues that it is impossible to determine bubble size from the amplitude since a reference value for the scattered signal produced by a bubble of known size cannot be obtained in an *in vivo* situation. Calculation of absolute size is almost impossible because it is necessary to know the attenuation by the different tissues, the distance of the bubble from the transducer, and the coupling loss at the transducer-tissue interface. Comparisons with *in vitro* experiments cannot be made unless all conditions are identical to those *in vivo*.

The use of two methods to determine the detection threshold for single gas bubbles for the pulse echo system used by ter Haar and Daniels have been reported (Beck et al., 1978; Daniels et al., 1979). In the first method, the minimum bubble diameter detected was plotted against receiver gain while the transducer was stationary. The second method employed simultaneous ultrasonic and microscopic observation of the decay of a gas bubble under a gelatin block. The relationship between image size and bubble size could not be determined using these methods.

3.4. Calibration of the Imaging System

The imaging system resolution is normally not as good as transducer (acoustic) resolution, since electronics and the display can degrade resolution. Isolated bubbles were used to

determine the resolution of the system. Acoustic coupling gel (Aquasonic 100, Peter Laboratories, Inc.) was placed in a mold constructed with two plexiglass supporting rings (inside diameter = 1 in.) and plastic membrane (Sealwrap, Borden, Inc.) secured to the supporting rings using o-rings fitted to the grooves etched around the circumference. Glass rods were inserted into the gel so that any air trapped in the gel as the rings are clamped together can be eliminated. The ring assembly was waterproofed using connector sealant tape, and kept at 10°C for several days to allow bubbles to coalesce and congregate at the tips of the glass rods, leaving the remainder of the ring bubble free to the unaided eye (Fig. 16). The ring assembly was scanned under an Olympus microscope at 10X magnification to identify relatively isolated bubbles between 10 and 50 microns. The bubble location was marked and the exact size was determined using a calibrated microscope micrometer (one division equaled 0.704 microns). The ring assembly was placed in degassed water at room temperature and positioned at the focal point of the transducer. The attenuation of the ultrasonic pulse echo unit was adjusted so that only highly reflecting interfaces were visible. The ring assembly was moved about during scanning using a three axis linear translator, and reflections from the gel were observed. The tilt and rotate controls were adjusted to obtain the best view of the bubble. These controls allow the sonographer to tilt the image about the line of sight and to rotate the image about the vertical axis. When a reflection could be attributed to the marked bubble. the sample was retained. The stability of the system over time was investigated by repeating the calibration

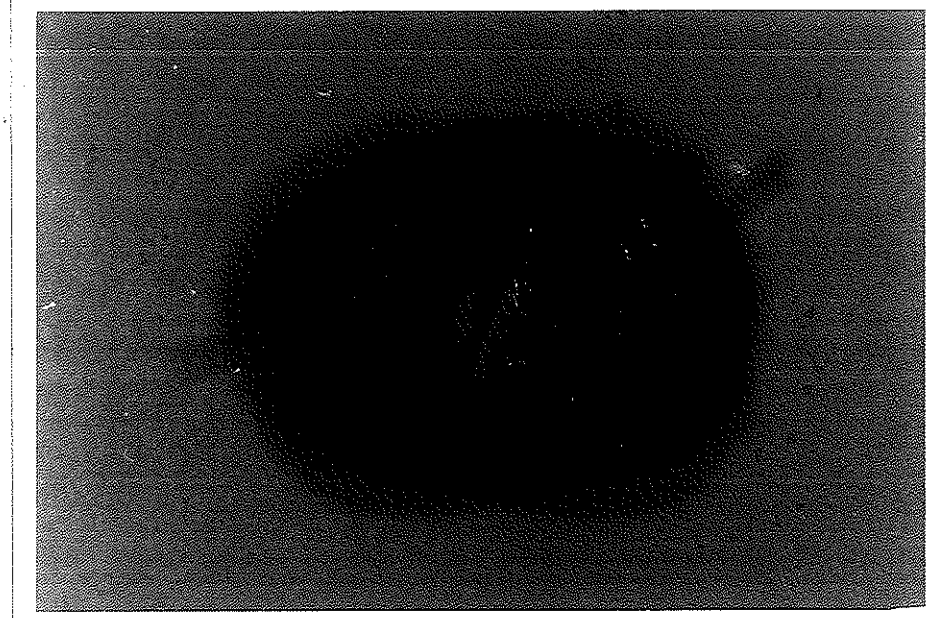

Figure 16. Ring assembly used to calibrate imaging system.

procedure several days later. The system was able to repeatedly resolve bubbles of 17 microns and larger. To resolve bubbles below this size, the attenuation of the unit had to be reduced to a level (less than 10 dB) which resulted in a low signal-to-noise ratio. Bubbles below the resolution of the system are described as silent.

A comparison of the specifications of the ter Haar and Daniels system and the newly developed system is given in Table 1. Although similarities between the two systems are evident, the differences in the irradiation frequency and intensity are worth noting. Since, in general, the cavitation threshold increases with increased frequency, the higher frequency employed in the current study is accompanied by higher intensities. Though the imaging systems have quite similar axial resolution, the 10 MHz imaging transducer has better lateral resolution as would be expected. However, if the radius of a focused acoustic beam in the focal plane, r_{focus}, is used to estimate the beamwidth, the lower frequency transducer seems to have better lateral resolution. The expression for r_{focus} as given by Gooberman (1968) is

$$r_{focus} = 0.61 \frac{\lambda f}{R} \qquad (3.7)$$

where f is the focal length and R is the radius of the transducer.

3.5. Data Aquisition System

Two wideband, high-speed amplifiers (Fig. 17), each with gains of 32 dB, have been developed to eliminate noise problems

TABLE 1

Comparison of Experimental Hardware

Irradiation Transducer	ter Haar/Daniels	U of I
frequency	0.75 MHz	1 MHz
diameter	2.5 cm	3.18 cm
distance to specimen	4.0 cm	11.8 cm
intensity range	80-680 mW/cm^2	89-289 W/cm^2
temperature	37°C	37°C, 10°C
Imaging Transducer		
frequency	8 MHz	10 MHz
diameter	5 mm	4 mm
focal distance	1.8 cm	2.5 cm
PRF	2 kHz	1.8 kHz
scan rate	1 Hz	18.5 Hz
SA/SP	1/3	~ 1/13
display magnification	1x, 2x, 4x	1x, 2x, 4x
radius of focal plane	0.82	1.14 mm
pulse duration	0.5 μs	0.5 μs
SPL	0.75 mm	0.75 mm
experimental beam width (3 dB)	1.6 mm	1.1 mm

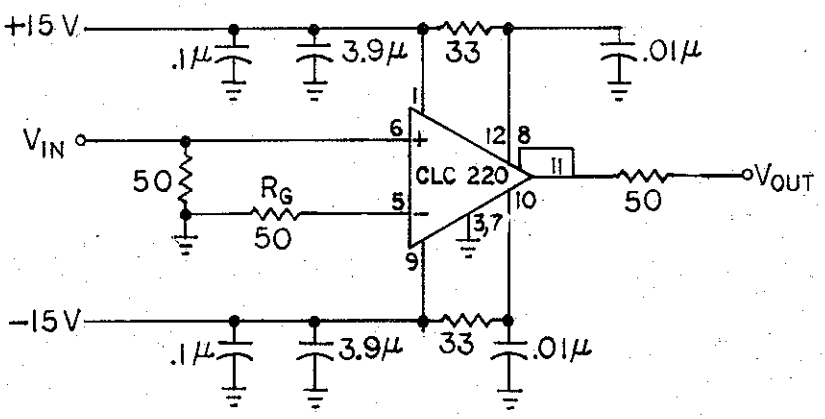

Figure 17. Pulse amplifier.

associated with the Hewlett-Packard model 461A wideband amplifier used previously in the data acquisition system developed by Morimoto (1984). The gain of the amplifier depends on the value of R_g when the internal 1500 Ω internal feedback resistor, R_f is used, and is given by

$$A_v = 1 + \frac{R_f}{R_g} \tag{3.8}$$

The maximum voltage into the amplifier is given by

$$V_{in}(max) = \frac{V_{cc} - 2.5}{Gain} = 0.4 \text{ v} \tag{3.9}$$

When designed for a gain of 30 dB, the amplifier (model CLC220AI, Comlinear Corporation) is reported to have a -3 dB bandwidth of 200 MHz, a 0.02% settling time of 10 ns, a 7000 V/μs slew rate, and a 2 ns rise and fall time for a 5 volt step. To assure optimum performance, lead lengths were kept to a minimum and a solid, unbroken ground plane was used.

Along with the amplifiers, a symmetrical π attenuator was built to optimize the gain (Fig. 18). The optimum gain is below the +/- 500 mv saturation level of the A/D converter. The A/D converter has a 50 MHz digitizing rate utilizing two TRW 25 MHz A/D's in parallel (Foster, 1984). The attenuation is variable from 1-21 dB, and is impedance matched to the coaxial cables (Z=50Ω) to prevent reflections. The values of R_1 and R_3 shown in Fig. 19 are chosen so that attenuations of 1, 2, 3, 6, and 9 dB and combinations thereof can be programmed by the operator. These values are selected to include the 1/2, 1/4, and 1/8 power attenuations. The design equations are

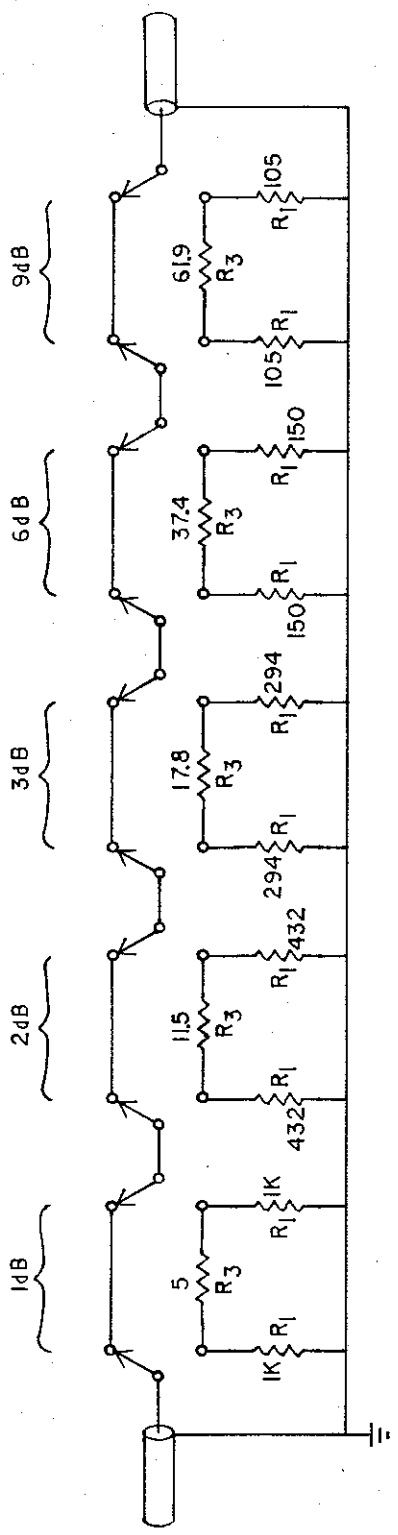

Figure 18. Attenuator.

$$\text{dB attenuation} = 20 \log N_v = 10 \log N$$

$$R_3 = Z[(N - 1)/2(N)^{1/2}] \qquad (3.10)$$

$$R_1 = Z[N^{1/2} + 1/(N^{1/2} - 1)]$$

where N_v and N are the voltage and power ratios, respectively. The measured attenuations using a Fluke 8920A True RMS Voltmeter and a Wavetek (Model 145, 20 MHz) Pulse/Function generator are given in Table 2. The attenuation which varies with frequency has a maximum attenuation at 10 MHz. The difference in attenuation is 0.34 and 1.64 dB for 1 and 21 dB attenuation settings, respectively, between 10 and 20 MHz.

TABLE 2

Measured Attenuation

Design Attenuation	Measured 1 kHz	1 MHz	10 MHz	20 MHz
1 dB	1.00	1.00	1.00	0.66
2	2.28	2.29	2.29	1.59
3	3.34	3.34	3.40	2.47
6	6.55	6.57	6.68	5.23
9	9.63	9.66	9.85	8.21
1+2	3.24	3.24	3.26	2.32
1+3	4.28	4.29	4.35	3.22
1+6	7.44	7.47	7.59	6.05
1+9	10.52	10.54	10.76	9.06
2+3	5.49	5.51	5.57	4.25
2+6	8.63	8.64	8.77	7.13
2+9	11.68	11.71	11.92	10.19
3+6	9.63	9.66	9.77	8.07
3+9	12.68	12.70	12.91	11.14
6+9	15.69	15.71	15.96	14.49
3+6+9	18.71	18.72	18.92	17.42
2+3+6+9	20.73	20.74	20.95	19.39
1+2+3+6+9	21.61	21.67	21.88	20.24

CHAPTER 4

PROCEDURE AND RESULTS

A preliminary examination was made of the images within the mouse neonate produced during and immediately after irradiation with high intensity 1 MHz ultrasound. The neonatal mice were acquired within 20 hours of birth from a large colony maintained within the Bioacoustics Research Laboratory. The neonates, whose average weight and length were 1.6 grams and 2.5 cm, respectively, were anesthetized by intramuscular injection of both Ketamine HCl and Xylazine at a dosage of 25-30 mg/kg. After anesthetization, the neonate was placed in a plexiglass holder equipped with air lines for breathing. The skin covering the dorsal was removed, and the holder was adjusted so that, when mounted in the tank, the third lumbar region of the neonate was centered on the 1MHz irradiation beam. In order for the imaging transducer unit to fit in the tank, the axial distance from the transducer to the neonate was increased by 2 cm relative to previous studies. Increasing the axial distance decreased the intensity by less than 2%. The imaging transducer unit was positioned such that its ultrasound beam was at 45^{o} to the 1MHz irradiation beam, and its focal region was centered on the spinal column (Fig. 19).

Results reported previously by Frizzell et al. (1983) suggest that cavitation begins to contribute significantly to hind limb paralysis of the neonate in the intensity range between 144 and 289 W/cm^2 at $10^{o}C$. At 289 W/cm^2 the exposure duration for paralysis in 50% of the animals exposed was nearly doubled

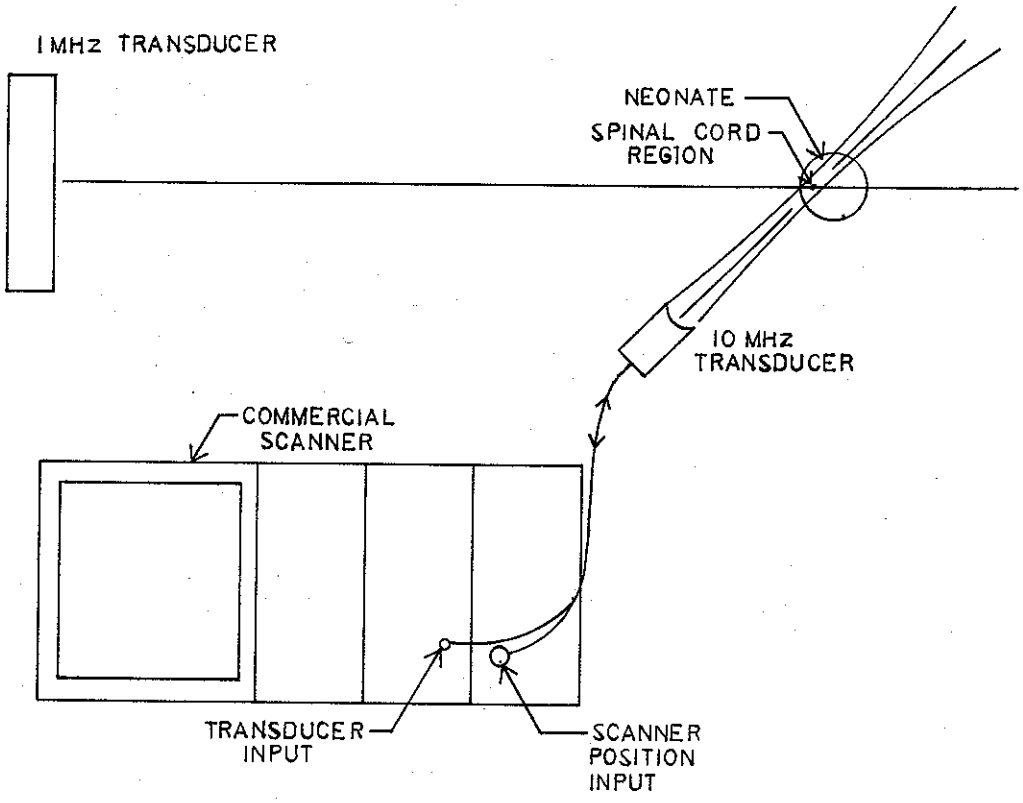

Figure 19. Transducer configuration during neonatal irradiation.

when the hydrostatic pressure was raised from 1 to 16 atmospheres, whereas no such change with pressure was observed at 144 W/cm^2 and lower (see the data from Frizzell et al. (1983) in Table 3). At elevated temperatures the cavitation threshold is lower so that cavitation might be expected to contribute at lesser intensity levels (Fry and Dunn, 1962). Thus, this initial imaging study was conducted at atmospheric pressure and 37^{o}C to provide a lower threshold condition for the onset of cavitation. The t_{90} values, the exposure time at each intensity where 90% of the neonates developed hind limb paralysis. at 10^{o}C were used to provide a guide for an irradiation time at each intensity to assure that cavitation activity will occur if it is going to.

A total of nine neonates were irradiated and examined using the imaging system discussed in Chapter 3, three each at intensities of 144, 192, and 230 W/cm^2 for 1.2, 0.6, and 0.5 seconds, respectively. It was necessary to examine the images immediately after the irradiation field was turned off to avoid picking up the harmonics associated with the irradiation field. Therefore, it was difficult to observe any changes and even more difficult to document them with the Polaroid oscilloscope camera (Model C-5C) used to make a permanent record. Of the nine animals examined, additional echoes surrounding the spinal cord were observed in only one animal exposed to 192 W/cm^2. Figures 20a and 20b (2X magnification) show the images of the mouse neonate produced by the imaging system and recorded by the camera without and with the additional echoes, respectively. These images were taken with the nosepiece removed from the imaging transducer, so that an attenuation of 40 dB could be employed,

TABLE 3

Exposure durations for hind limb paralysis in 10%, 50%, and 90% of specimens at 1 MHz, 10^6C, and the indicated intensities

I(w/cm2)	P(atm)	t_{10}(s)	t_{50}(s)	t_{90}(s)
86	1	3.44	5.04	9.40
86	16	2.59	4.50	18.70
105	1	2.01	2.56	3.53
122	1	1.37	1.53	1.72
144	1	0.84	0.97	1.14
144	16	0.85	0.97	1.12
192	1	0.36	0.44	0.58
256	1	0.23	0.30	0.45
289	1	0.20	0.26	0.37
289	16	0.30	0.50	1.54

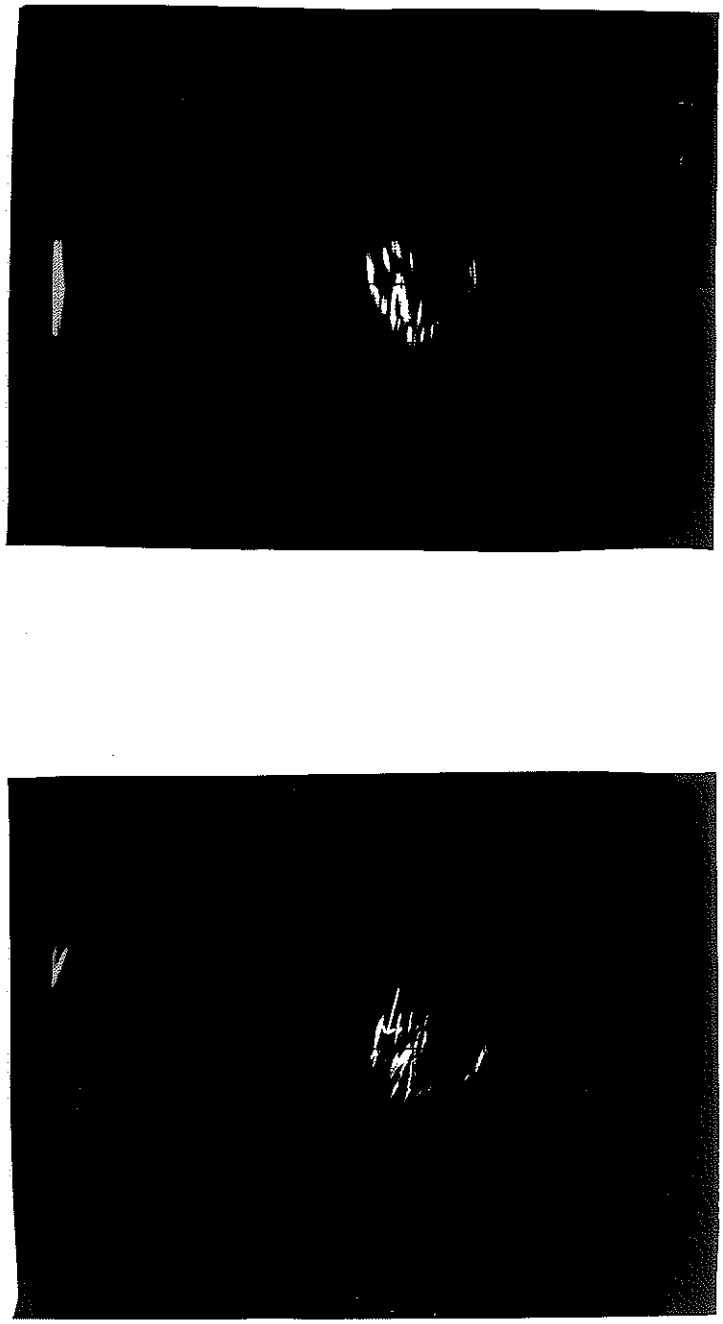

Figure 20. Ultrasonic image of mouse neonate without (A) and with (B) echoes in spinal cord region.

thereby minimizing noise and harmonic interference. The echoes are clearly visible surrounding the spinal cord, as indicated in the figure. These initial results suggest that there may have been bubbles produced at 192 W/cm^2. However, the fact that similar changes were not observed in the other animals exposed at 192 W/cm^2 and those exposed at 230 W/cm^2 raise questions about the reproducibility of this phenomenon and/or the recording technique employed. It is also possible that the additional echoes observed were associated with changes in temperature and differential change in impedance in the structures within the region of the spinal cord. Thus it is clear that many more animals need to be examined, and that the recording techniques need to be improved, as discussed in Chapter 5.

CHAPTER 5

RECOMMENDATIONS AND CONCLUSIONS

5.1. Recommedations for Future Research

The work by Frizzell et al. (1983) was important in that it demonstrated a shift in threshold with a change in hydrostatic pressure at 289 W/cm^2, which indicated involvement of a cavitation mechanism of damage. However, studies of the effect of pressure at 10^oC at intensities between 144 and 289 W/cm^2 are needed to better determine the lowest intensity at which the shift seems to occur. A similar study should also be performed at 37^oC in order to determine the effect of temperature on the cavitation threshold. The temperature rise in the spinal cord should be monitored during the 37^oC irradiations so that any thermal mechanism of damage can be ruled out. The effect of increased absorption, and therefore temperature, due to the bubbles, should be investigated during irradiations under pressurized and atmospheric conditions.

The imaging system could be improved by the addition of high quality video equipment with slow motion capability. The irradiation procedure could then be documented and reviewed for the presence of cavitation activity in the form of "visible" bubbles. Currently this activity is determined in a fraction of a second by the subjective judgement of the sonographer during real time viewing. The Polaroid camera is inadequate in that there is a low probability that the hard copy will be initiated at the instant the irradiation field is turned off. A higher resolution 15 MHz transducer is available if need is established

from the recommended studies. However, the increased complexity of the signal processing hardware at the higher frequency prohibits its use for anything but qualitative evaluation.

5.2. Conclusions

A 10 MHz commercial opthalmic ultrasound scanner was modified and calibrated for imaging the mouse neonate to determine if bubbles are produced during irradiation with high intensity 1 MHz ultrasound. A preliminary study using this bubble imaging system showed echoes in one specimen that may have been associated with bubble activity in the mouse neonate. However, more studies are required to determine if the echoes were associated with bubbles as opposed to other phenomena. As with the ter Haar and Daniels study, the resolution of the system is above the resonant size bubble, so that any bubbles visualized must have grown considerably by rectified diffusion. Interference from the harmonics associated with the irradiation beam was found to be the largest obstacle to visualizing bubbles during irradiation.

The acquisition of a video camera should aid substantially the visualization of any bubble activity in the mouse neonate produced by the 1 MHz ultrasonic irradiation.

REFERENCES

Akulichev,V.A. (1966). "Hydration of Ions and the Cavitation Resistance of Water," Sov. Phys. Acoust. 12, 144-149.

Alexander, P. and Fox, M. (1954). J. Polymer Sci. 12, 533.

Apfel, R. E. (1970). "The Role of Impurities in Cavitation Threshold Determination," J. Acoust. Soc. Am. 48, 1179-1189.

Apfel, R. E. (1981). "Acoustic Cavitation" in Methods of Experimental Physics, P.E. Edmonds, ed., (Academic Press, New York), 19, 355-411.

Apfel, R. E. (1982). "Acoustic Cavitation: A Possible Consequence of Biomedical Uses of Ultrasound," Br. J. Cancer, 45, Suppl. V, 140-146.

Apfel, R. E. (1986). "Possibility of Microcavitation from Diagnostic Ultrasound," IEEE Trans. Ultrason., Ferroelect.. and Freq. Control, Special Issue on Bioeffects (to be published).

Aschenbach, P. D. (1982). MS Thesis, University of Illinois, Urbana, Illinois.

Atchley. A. A. (1985). "The Nucleation of Cavitation in Aqueous Media," Ph.D. Thesis, University of Mississippi, Oxford, MS.

Beck, T. W., Daniels, D., Paton, W. D. M. and Smith, E. B. (1978). "The Detection of Bubbles in Decompression Sickness," Nature 276, 173.

Berg, R. B.. Child, S. Z. and Carstensen, E. L. (1983). "The Influence of Carrier Frequency on the Killing of

Drosophila Larvae by Microsecond Pulses of Ultrasound," Ultrasound Med. Bio. 9, L448-L451.

Blake, F. G. (1949). "The Onset of Cavitation in Liquids," Tech. Mem. No. 12, Acoustic Research Laboratory, Harvard University, Cambridge, Massachusetts.

Carstensen, E. L. (1985). Presentation at conference held at University of Rochester, May, 1985.

Carstensen, E. L. and Child, S. Z. (1980). "Effects of Ultrasound on Drosophila--II: The Heating Mechanism," Ultrasound Med. Bio. 6, 257-261.

Carstensen, E. L., Child, S. Z. Law, W. K., Horowitz, D. R. and Miller, M. W. (1979). "Cavitation as a Mechanism for the Biological Effects of Ultrasound on Plant Roots," J. Acoust. Soc. Am. 66, 1285-1291.

Carstensen, E. L., Child, S. Z., Lam, S., Miller, D. L. and Nyborg, W. L. (1983). "Ultrasonic Gas Body Activation in Drosophila," Ultrasound Med. Biol. 9, 473-477.

Carstensen, E. L., Donaldson, T. L., Miller, M. W., Law, W. K. and Vives, B. (1981). "Distribution of Gas in the Roots of Pisum Sativum," Environmental and Experimental Bot. 21, 1-4.

Carstensen, E. L. and Flynn, H. G. (1982). "The Potential for Transient Cavitation with Pulsed Ultrasound," Ultrasound Med. Bio. 8, 720-724.

Carstensen E. L. and Gates A. H. (1984). "The Effects of Pulsed Ultrasound on the Fetus," J. Ultrasound Med. 3,145-147.

Chan, S. and Frizzell, L. A. (1977). "Ultrasonic Thresholds for Structural Changes in the Mammalian Liver," Proc. IEEE Sonics Ultrasonics Symp., Cat. 77CH1264-ISU, 153-156.

Chapelon, J. Y., Shankar, P. M. and Newhouse, V. L. (1985). "Ultrasonic Measurement of Bubble Cloud Size Profiles," J. Acoust. Soc. Am. 78, 196-201.

Child, S. Z.,Carstensen, E. L. and Miller, M. W. (1975). "Growth of Pea Roots Exposed to Pulsed Ultrasound," J. Acoust. Soc. Am. 53, 1109-1110.

Child, S. Z., Carstensen, E. L. and Smachlo, K. (1980). "Effects of Ultrasound on Drosophila--I: Killing of Eggs Exposed to Traveling and Standing Wave Fields," Ultrasound Med. Bio. 6, 127-130.

Child, S. Z., Carstensen, E. L. and Lam, S. K. (1981). "Effects of Ultrasound on Drosophila--III: Exposure of Larvae to Low-Temporal-Average-Intensity, Pulsed Irradiation," Ultrsound Med. Bio. 7, 167-173.

Child, S. Z. and Carstensen, E. L. (1982). "Effects of Ultrasound on Drosophila--IV: Pulsed Exposures of Eggs," Ultrasound Med. Bio. 8, 311-312.

Coakley, W. T. and Dunn, F. (1971). "Degradation of DNA in High-Intensity Focused Ultrasonic Fields at 1 MHz," J. Acoust. Soc. Am. 50, 1539-1545.

Coakley, W. T., Hampton, D. and Dunn, F. (1971). "Quantitative Relationships between Ultrasonic Cavitation and Effects Upon Amoebae at 1 MHz," J. Acoust. Soc. Am. 50, 1546-1553.

Coakley, W. T. and Nyborg, W. L. (1978). "Cavitation: Dynamics of Gas Bubbles; and Applications," Chapter II in Ultrasound: Its Application in Medicine and Biology, F. J. Fry, ed., (Elsevier Publishing Co., New York).

Counce, S. J. and Selman, G. G. (1955). "The Effects of Ultrasonic Treatment and Embryonic Development of Drosophila melangaster," J. Embryol. Exp. Morphol. 3, 121-141.

Crum, L. A. (1980). "Measurements of the Growth of Air Bubbles by Rectified Diffusion," J. Acoust. Soc. Am. 68, 203-211.

Crum, L. A. (1984). "Rectified Diffusion," Ultrasonics 22, 215-223.

Crum, L. A. (1982). "Nucleation and Stabilization of Microbubbles in Liquids," Appl. Sci. Res. 38, 88-101.

Crum, L. A. (1985). Presentation at conference held at University of Rochester, May, 1985.

Crum, L. A. and Hanson, G. M. (1982). "Generalized Equations for Rectified Diffusion," J. Acoust. Soc. Am. 75, 1586-1592.

Daniels, S., Paton, W. D. M. and Smith, E. B. (1979). "Ultrasonic Imaging System for the Study of Decompression Induced Gas Bubbles," Undersea Biomedical Research 6, 197-207.

Daniels, S., Davies, J. M.,Paton, W. D. M. and Smith, E. B. (1980). "The Detection of Gas Bubbles on Guinea Pigs After Decompression From Air Saturated Dives Using Ultrasonic Imaging," J. Physiol. 308, 369-383.

Dooley, D. A., Child, S. Z., Carstensen, E. L. and Miller, M. W. (1983). "The Effects of Continuous Wave and Pulsed Ultrasound on Rat Thymocytes In Vitro," Ultrasound Med. Bio. 9, 379-384.

Dunn, F. (1956). Ph. D. Thesis, University of Illinois, Urbana, IL.

Dunn, F. (1982). "Selected Biological Effects of Ultrasound," in Essentials of Medical Ultrasound, M. Repacholi, ed., 4, 117-140 (Humana Press).

Dunn, F. and Fry, F. J. (1971). "Ultrasonic Threshold Dosages for the Mammalian Central Nervous System," IEEE Trans. Bio-Med. Eng. BME-18, 253-256.

Dunn, F. and Fry, W. J. (1957). "An Ultrasonic Dosage Study: Functional Endpoint," in Ultrasound in Bio. and Med.. E. Kelly, ed., (Amer. Inst. Biolog. Sciences, Washington, D.C.), 226-235.

Dunn, F. and O'Brien W. D., Eds. (1976). Ultrasonic Biophysics, (Dowden, Hutchinson, and Ross, Inc., Stroudsburg, Pa.).

Eames, F. A., Carstensen, E. L., Miller, M. W. and Li, M. (1975). "Ultrasonic Heating of Vicia faba Roots," J. Acoust. Soc. Am. 57, 1192-1194.

Eller, A. I. and Flynn, H. G. (1965). "Rectified Diffusion During Nonlinear Pulsation of Cavitation Bubbles," J.

Acoust. Soc. Am. 37, 493-503.

Evans, A. (1977). "Some Limiting Factors in Ultrasonic Bubble Detection in vivo," in Early Diagnosis of Decompression Sickness, R. Pearson, ed.. Undersea Medical Society, Bethesda, 69-80.

Flynn, H. G. (1964). "Physics of Acoustic Cavitation in Liquids," in Physical Acoustics, Vol. 1B, W. P. Mason, ed., (Academic Press, New York).

Flynn, H. G. (1982). "Generation of Transient Cavities in Liquids by Microsecond Pulses of Ultrasound," J. Acoust. Soc. Am. 72, 1926-1932.

Foster, S. G. (1984). Ph. D. Thesis, University of Illinois, Urbana, Illinois.

Fox, F. E. and Herzfeld, K. F. (1954) J. Acoust. Soc. Am. 26, 985.

Fritz-Niggli, H. and Boni, A. (1950). "Biological Experiments on Drosophila melanogaster with Supersonic Vibrations," Science 111, 120-122.

Frizzell, L. A., Lee, C. S.. Aschenbach, P. D., Borelli, M. J., Morimoto, R. S. and Dunn, F. (1983). "Involvement of Ultrasonically Induced Cavitation in the Production of Hind Limb Paralysis of the Mouse Neonate," J. Acoust. Soc. Am. 74, 1062-1065.

Fry, F. J. (1978). Ultrasound: Its Application in Medicine and Biology, (Elsevier Publishing Co., New York).

Fry, F. J., Kossoff, G., Eggleton, R. C. and Dunn, F. (1970). "Threshold Ultrasonic Dosages for Structural Changes in Mammalian Brain," J. Acoust. Soc. Am. 48, 1413-1417.

Fry, W. J. and Dunn, F. (1962). "Ultrasound: Analysis and Experimental Methods in Biological Reseach," Chapter VI in Physical Techniques in Biological Research, W.L. Nastuk, ed., (Academic Press, New York), 4, 261-394.

Fry, W. J., Tucker, D., Fry, F. J. and Wulff, V. J. (1951). "Physical Factors Involved in Ultrasonically Induced Changes in Living Systems: II. Amplitude Duration Relations and the Effect of Hydrostatic Pressure for Nerve Tissue," J. Acoust. Soc. Am. 23, 364-368.

Fulton, J. F. (1951). Decompression Sickness (W.B. Saunders Co., Philadelphia).

Gooberman, G. (1960). J. Polymer Sci. 42, 25.

Gooberman, G. (1968). Ultrasound: Theory and Application, (English Univ. Press, London).

Gould, R. K. (1974). J. Acoust. Soc. Am. 56, 1740.

Gramiak, R. and Shah, P. M. (1971). "Detection of Intracardiac Blood Flow by Pulsed Echo Imaging Ultrasound," Radiology 100, 415-418.

Harvey, E. N. (1951). in Decompression Sickness, J.F. Fulton, ed., (W.B. Saunders, Philadelphia), Chapter IV.

Harvey, E. N. and Loomis, A. L. (1928). "High Frequency Sound Waves of Small Intensity and their Biological Effects," Nature 121, 622-624.

Harvey, E. N., Barnes, D. K., McElroy, W. D., Whitely, A. H., Pease, D. C. and Cooper, K. W. (1944). "Bubble

Formation in Animals," J. Cell Comp. Physiol. 24, 23.

Hemmingsen, E. A. (1982). J. Exp. Zool. 220, 43.

Herzfeld, K. F. (1957). Comment in Proc. First Sympos. Naval Hydrodyn., (Nat. Acad. Sci., Wash. D.C.), F.S. Sherman, ed., pp. 319-320.

Hill, C. R., Clarke, P. R., Crowe, M. and Hammik, J. W. (1969). Ultrasonics for Industry Papers (Iliffe Ind. Pub., London), 26.

Hills, B. A. and Grulke, D. C. (1975). "Evaluation of Ultrasonic Bubble Detectors in vitro Using Calibrated Microbubbles at Selected Velocities," Ultrasonics 13, 181-184.

Hsieh, D. Y. and Plesset, M. D. (1961). J. Acoust. Soc. Am. 33, 206.

Kremkau, F. W. (1984). Diagnostic Ultrasound: Principles, Instrumentation, and Exercises, (Grune and Stratton, Inc., Orlando, FL.).

Lee, C. S. (1982). MS Thesis, University of Illinois, Urbana, Illinois.

Lele, P. P. (1975). "Ultrasonic Teratology in Mouse and Man," in Proc. Second European Congress on Ultrasonics in Medicine (ISBN 90 219 0297 4).

Lele, P. P. (1977). "Thresholds and Mechanisms of Ultrasonic Damage to Organized Animal Tissues," in Proc. Symp. Bio. Effects and Characterizations of Ultrasound Sources, D.W.G. Hazard and M.L. Litz, eds., (HEW Publication (FDA) 78-8048), 224-239.

Lele, P. P. (1978). "Cavitation and its Effects on Organized

Mammalian Tissues," in Ultrasound: Its Application in Medicine and Biology, F.J. Fry, ed., (Elsevier Scientific, New York), App. I, 737-741.

Mackay, R. S. (1963). Discussion Remark in Proc. Second Symp. Underwater Physio., C.J. Lambertsen and L.J. Greenbaum, Jr., eds.. Publ. No. 1181 (Nat. Acad. Sci.- Nat. Res. Council. Washington D.C.), 41.

Mackay, R. S. and Rubissow, G. J. (1971). "Detection of Bubbles in Tissues and Blood," in Proc. Fourth Symp. Underwater Physiology, C. J. Lambertsen, ed., 151-160.

McKee, J. R.. Christman, C. L., O'Brien, W. D. and Wang, S. Y. (1977). "The Effects of Nucleic Acid Bases," Biochem. 16, 4651-4654.

Miller, D. L. (1977). "The Effects of Ultrasonic Activation of Gas Bodies in Elodea Leaves During Continuous and Pulsed Irradiations at 1 MHz," Ultrasound Med. Bio. 3, 221-240.

Miller, D. L. (1979a). "A Cylindrical Bubble Model for the Response of Plant-Tissue Gas Bodies to Ultrasound," J. Acoust. Soc. Am. 65, 1313-1321.

Miller, D. L. (1979b). "Cell Death Thresholds in Elodea for 0.45-10 MHz Ultrasound Compared to Gas-Body Resonance," Ultrasound Med. Bio. 5, 351-357.

Miller, D. L. (1980). "Acoustic Interaction of Spherical and Cylindrical Bubbles on Plane Sheets and Ribbons," Ultrasonics 18, 277-282.

Miller, D. L. (1983a). "Further Examination of the Effects of Ultrasonic Activation of Gas Bodies in Elodea Leaves," Env. Exp. Bot. 23, 393-405.

Miller, D. L. (1983b). "The Botanical Effects of Ultrasound: A Review," Envir. and Exp. Bot. 23, 1-27.

Miller, D. L. (1984). "Gas Body Activation," Ultrasonics, Nov., 261-269.

Miller, D. L. and Nyborg, W. L. (1983). "Theoretical Investigation of the Response of Gas-Filles Micropores and Cavitation Nuclei to Ultrasound," J. Acoust. Soc. Am. 73, 1537-1544.

Miller, D. L., Nyborg, W. L. and Whitcomb, C. C. (1978). "In vitro Clumping of Platelets Exposed to Low Intensity Ultrasound," in Ultrasound on Medicine, D. White and E.A. Lyons, eds., (Plenum, New York), Vol. 4, 545-553.

Miller, D. L. and Williams, A. R. (1983). "Further Investigations of ATP Release From Human Erythrocytes Exposed to Ultrasonically Activated Gas-Filled Pores," Ultrasound Med. Bio. 9, 297-307.

Miller, M. W., Voorhees, S. M., Carstensen, E. L. and Eames, F. A. (1974). "An Histological Study of the Effect of Ultrasound on the Growth of Vicia faba Roots," Radiar. Bot. 14, 201-206.

Morimoto, R. S. (1984). MS Thesis, University of Illinois, Urbana, Illinois.

National Council on Radiation Protection and Measurements (NCRP) Report (1983). "Biological Effects of Ultrasound: Mechanisms and Clinical Implications," No. 74.

Neppiras, E. A. (1980). "Acoustic Cavitation," Physics Reports, 61, 159-251.

Neppiras, E. A. and Noltink, B. E. (1951). Proc. Phys.

Soc. (London), B64, 1032.

Nishi, R. Y. (1977). "Problem Areas in the Ultrasonic Detection of Decompression Bubbles," in Early Diagnosis of Decompression Sickness, Undersea Medical Society, Bethesda, 50-68.

Nyborg, W. L. (1965). "Acoustic Streaming" in Physical Acoustics, Vol. IIB, W.P. Mason, ed., (Academic Press, New York), 256-331.

Nyborg, W. L. (1978). "Physical Mechanisms for Biological Effects of Ultrasound," DHEW Publication (FDA) 78-8062, Bureau of Radiological Health, Rockville, MD.

Nyborg, W. L., Miller, D. L. and Gershoy, A. (1976). "Physical Consequences of Ultrasound in "Plant Tissues and other Bio-Systems," in Fundemental and Applied Aspects of Nonionizing Radiation, S.M. Michaelson and M.W. Miller, eds., (Plenum Press, New York), 277-299.

O'Brien, W. D., Januzik, S. J. and Dunn, F. (1982). "Ultrasound Biologic Effects: A Suggestion of Strain Specificity," J. Ultrasound Med. Bio. 1, 367.

O'Brien, W. D. (1976). "Ultrasonically Induced Fetal Weight Reduction in Mice," in Ultrasound in Medicine, D. White and R. Barnes, eds., (Plenum Press, New York), 2, 531.

O'Brien, W. D. (1983). "Dose-dependent Effect of Ultrasound on Fetal Weight in Mice," J. Ultrasound Med. 2, 1.

Pay, T. L., Anderson, F. A. and Jessup, G. L. (1978). "Survival of Drosophila melanogaster Pupa Exposed to Ultrasound," Rad. Res. 75, 236-241.

Pond, J. B. (1970). "The Role of Heat in the Production of

Ultrasonic Focal Lesions," J. Acoust. Soc. Am. 47, 1607-1611.

Robinson, T. C. and Lele, P. P. (1972). "An Analysis of Lesion Development in the Brain and in Plastics by High Intensity Focused Ultrasound at Low Megahertz Frequencies," J. Acoust. Soc. Am. 51, 1333.

Rubissow, G. J. and Mackay, R. S. (1974). "Decompression Study and Control Using Ultrasonics," Aero. Med. 45, 473-478.

Schmitt, F. and Uhlemeyer, B. (1930). "The Mechanisms of Lethal Effects of Ultrasonic Radiation," Proc. Soc. Exp. Bio. Med. 27, 626.

Selman, G. G. and and Counce, A. (1953). "Abnormal Embryonic Development in Drosophila Induced by Ultrasonic Treatment," Nature 172, 503-504.

Shoji, R., Momma, F., Shimizu, T. and Matsuda, S. (1972). "Experimental Studies on the Effect of Ultrasound on Mouse Embryos," Teratology 6, 119.

Sirotyuk, M. G. (1970). "Stabilization of Gas Bubbles in Water," Sov. Phys. Acoust. 16, 237-240.

Strasberg, M. (1959). "Onset of Ultrasonic Cavitation in Tap Water," J. Acoust. Soc. Am. 31, 163-176.

Strasberg, M. (1961). J. Acoust. Soc. Am. 33, 359.

ter Haar, G. and Daniels, S. (1981). "Evidence for Ultrasonically Induced Cavitation in vivo," Phys. Med. Bio. 26, 1145.

ter Haar, G. R., Daniels, S., Eastaugh, K. C. and Hill, C. R. (1982). "Ultrasonically Induced Cavitation in vivo," Br.

J. Cancer 45, Supp. V, 151.

ter Haar, G. R. Dyson, M. and Smith, S. (1979). Ultrasound Med. Bio. 5, 167-179.

Van Liew, H. D. (1968). Am. J. Physiology, 214, 1176.

Van Liew, H. D. and Passke, M. (1967). Aerosp. Med. 38, 829.

Wells, P. N. T. (1984). "Medical Ultrasonics," IEEE Spectrum, 21, No. 12, 44-51.

Williams, A. R. and Miller, D. L. (1980). "Photometric Detection of ATP Release from Humane Erythrocytes Exposed to Ultrasonically Activated Gas Filled Pores," Ultrasound Med. Bio. 6, 251-256.

Wood, R. W. and Loomis, A. L. (1927). "The Physical and Biological Effects of High Frequency Sound Waves of Great Intensity," Phil. Mag. 6, 417.

Yount, D. E. (1979). "Skins of Varying Permeability: A Stabilization Mechanism for Gas Cavitation Nuclei," J. Acoust. Soc. Am. 65, 1429.

Yount, D. E., Gillary, E. W. and Hoffman, D. L. (1984). "A Microscopic Investigation of Bubble Formation Nuclei," J. Acoust. Soc. Am. 76, 1511-1521.